12-1-2020

ANALYZING THE STREAMFLOW FOR FUTURE FLOODING AND RISK ASSESSMENT UNDER CMIP6 CLIMATE PROJECTION

Indira Pokhrel
Southern Illinois University Carbondale, indirapokhrel12@gmail.com

ANALYZING THE STREAMFLOW FOR FUTURE FLOODING AND RISK ASSESSMENT UNDER CMIP6 CLIMATE PROJECTION

by

Indira Pokhrel

B.E., Tribhuvan University, 2017

A Thesis

Submitted in Partial Fulfillment of the Requirements for the

Master of Science Degree

Department of Civil and Environmental Engineering
in the Graduate School
Southern Illinois University Carbondale
December 2020

THESIS APPROVAL

ANALYZING THE STREAMFLOW FOR FUTURE FLOODING AND RISK ASSESSMENT UNDER CMIP6 CLIMATE PROJECTION

by

Indira Pokhrel

A Thesis Submitted in Partial

Fulfillment of the Requirements

for the Degree of

Master of Science

in the field of Civil Engineering

Approved by:

Dr. Ajay Kalra, Chair

Dr. Bruce A. DeVantier

Dr. Trent W. Ford

Graduate School
Southern Illinois University Carbondale
September 24, 2020

AN ABSTRACT OF THE THESIS OF

Indira Pokhrel, for the Master of Science degree in Civil Engineering, presented on September 24, 2020, at Southern Illinois University Carbondale.

TITLE: ANALYZING THE STREAMFLOW FOR FUTURE FLOODING AND RISK ASSESSMENT UNDER CMIP6 CLIMATE PROJECTION

MAJOR PROFESSOR: Dr. Ajay Kalra

Hydrological extremes associated with climate change are becoming an increasing concern all over the world. Frequent flooding, one of the extremes, needs to be analyzed while considering climate change to mitigate flood risk. This study forecasted streamflow and evaluated the risk of flooding in the Neuse River, North Carolina considering future climatic scenarios, and comparing them with an existing Federal Emergency Management Agency (FEMA) flood insurance study (FIS) report. The cumulative distribution function transformation (CDF-t) method was adopted for bias correction to reduce the uncertainty present in the Coupled Model Intercomparison Project Phase 6 (CMIP6) streamflow data. To calculate 100-year and 500-year flood discharges, the Generalized Extreme Value (GEV) (L-Moment) was utilized on bias-corrected multimodel ensemble data with different climate projections. The delta change method was applied for the quantification of flows, utilizing the future 100-year peak flow and FEMA 100-year peak flows.

Out of all projections, shared socio-economic pathways (SSP)5-8.5 exhibited the maximum design streamflow, which was routed through a hydraulic model, the Hydrological Engineering Center's River Analysis System (HEC-RAS), to generate flood inundation and risk maps. The result indicates an increase in flood inundation extent compared to the existing study, depicting a higher flood hazard and risk in the future. This study highlights the importance of

forecasting future flood risk and utilizing the projected climate data to obtain essential information to determine effective strategic plans for future floodplain management.

ACKNOWLEDGMENTS

I would like to extend my deepest gratitude to Dr. Ajay Kalra, my thesis advisor, for his guidance, supervision, and mentorship throughout my graduate study. The assistance that he provided was pivotal to the success of this research.

I would like to acknowledge Dr. Bruce A. DeVantier and Dr. Trenton Ford for the help and advice they offered not only during my research but also whilst serving on my thesis committee. My special thanks go to MD Mafuzur Rahaman, former student of SIUC who helped me to outline the research. I would like to thanks to Neekita Joshi, Balbhadra Thakur, Alen Shrestha, Rohit Jogineedi for being lab partner and resolving issues that were encountered during research. I owe my thanks to the IT staff for their continuous help in installing software and fixing any issues encountered thereof. I am particularly thankful to Ms. Jennifer Langin for her support and guidance throughout the starting my master's study.

I would like to express my sincere thanks to my parents, siblings, friends, and colleagues for their love, patience, and advice in different aspects of life. I would like to express my deepest appreciation to the entire faculty, staff, and colleagues of the Southern Illinois University's Civil and Environmental Engineering Department for their help and guidance throughout my graduate study.

I would like to dedicate this thesis to my loving father, Surya Prasad Pokhrel, mother, Bhagwati Poudel, and husband, Santosh Shrestha for their love, support, and continuous motivation, which helped me to achieve the goal.

I wish to thank FEMA for providing the data used in this paper. I acknowledge the modeling groups, the Program for Climate Model Diagnosis and Intercomparison, and the World

Climate Research Programme (WCRP) Working Group on Coupled Modelling for their roles in making available the WCRP CMIP6 multi-model dataset.

TABLE OF CONTENTS

CHAPTER PAGE

ABSTRACT i

ACKNOWLEDGMENTS iii

LIST OF TABLES vii

LIST OF FIGURES viii

CHAPTERS

CHAPTER 1 INTRODUCTION 1

1.1. Background 1

1.2. Problem Statement and Objective 3

1.3. Approach 5

1.4. Thesis Organization 6

CHAPTER 2 LITERATURE REVIEW 7

2.1 Introduction 7

2.2 Climate Change 11

2.3 Climate Change Projection 11

2.3.1 GCMs for Climate Projection 12

2.3.2 Climate Scenarios 12

2.3.3 Bias Correction of GCM 14

2.4 Flood Frequency Analysis 15

2.5 HEC-RAS Model 16

2.6 Floodplains Inundation Mapping and Risk Assessment 17

CHAPTER 3 STUDY AREA AND DATA 19

3.1 Study Area 19
3.2 Input Data 21
CHAPTER 4 METHODOLOGY 26
4.1 Statistical Analysis 27
4.1.1 Bias Correction 27
4.1.2 Quantification of the Future Design Flow 29
4.2 Hydraulic Modeling 30
4.3 Hazard and Risk Classification 31
CHAPTER 5 RESULT AND DISCUSSION 37
5.1 Flood Frequency Analysis and Performance of Hydraulic Modeling 37
5.2 Flood Inundation Mapping 42
5.3 Risk Zone Assessment and Mapping 51
5.4 Discussion 57
CHAPTER 6 SUMMARY AND CONCLUSION 61
6.1 Summary and Conclusion 61
6.2 Limitations 63
CHAPTER 7 RECOMMENDATION FOR FUTURE WORKS 64
REFERENCES 65
VITA 87

LIST OF TABLES

TABLE PAGE

Table 1: Scenarios in CMIP6 with their forcing level and SSPs 14

Table 2: Major Hurricanes that cause flooding in Neuse River and its fatalities inside US..... 21

Table 3: Climate projections for historical and future scenarios used in the study along with their number of ensemble members and modeling institute. 22

Table 4: Land Use and Land Cover 2016 with assigned Manning's Coefficient 24

Table 5: Summary of discharge (m3/s) at USGS gage site 02089500, downstream of study reach given by FFR. 24

Table 6: Flood hazard classification and its description considering water depth as an indicator of the degree of hazard. 33

Table 7: Reclassification of the land use data obtained from NLCD (2016) for the study area near Kinston with their assigned value for vulnerability assessment. 35

Table 8: Zonal Classification of flood risk based on the severity..... 36

Table 9: DCF values for future scenarios with 100-year and 500-year return period 40

Table 10: Hazard extent for the 100-year and 500-year return period flood events for both existing FEMA and future scenarios, respectively. 47

Table 11: Flood risk extent based on the zonal risk classification for 100-year and 500-year return period flood event for existing and future scenarios, respectively. 52

LIST OF FIGURES

FIGURE PAGE

Figure 1: Illustrative figure showing the scenario formation in CMIP6 13

Figure 2: Description of Cross-section in main channel 17

Figure 3: (a) States boundaries outlining counties of North Carolina (NC) including Kinston City, (b) Lenoir county showing the Kinston City at downstream of the study reach, (c) existing information of the study area from a FEMA flood insurance study (FIS) report (FFR) cross-sections and their labels along with their elevation. 20

Figure 4: Schematic diagram showing the sequential steps followed to analyze flood frequency, predict the future streamflow, flow routing, floodplain mapping, and risk assessment. 26

Figure 5: Illustrative figure showing bias correction using CDF-t methods. 28

Figure 6: Reclassified NLCD map for the vulnerability assessment 34

Figure 7: Annual peak streamflow for (a) historical observation data and (b) different future scenarios 38

Figure 8: Box plot for the comparison of different future scenarios DCF using different recurrence intervals 40

Figure 9: Calibration plot of FFR given WSEL versus Simulated WSEL 42

Figure 10: Comparison of flood extent map of Neuse River using the ArcMap (Version 10.7.1) between FEMA and future scenarios for (a) 100-year and (b) 500-year return period flood events, respectively. 44

Figure 11: Comparison of flood characteristics such as flood extent, channel velocity, and top width for different flooding scenarios considering (a) 100-year and (b) 500-year return period flood events, respectively..... 46
Figure 12: A Comparison of extent of flood hazard utilizing different flooding scenarios, i.e., FEMA and Future, respectively for 100 return period flood events..... 49
Figure 13: A Comparison of extent of flood hazard utilizing different flooding scenarios, i.e., FEMA and Future, respectively for 500-year return period flood events..... 50
Figure 14: Comparison of extent of risk for 100-year a) existing (FEMA) and b) future scenarios utilizing the risk zonal classifications 54
Figure 15: Comparison of extent of risk for 500-year a) existing (FEMA) and b) future scenarios utilizing the risk zonal classifications. 56

CHAPTER 1

INTRODUCTION

1.1 Background

Water is important for the survival of every living being in the world. For the proper allocation of water resources in a sustainable way, water resources management is considered as an important factor. The availability and accessibility of water resources can directly affect the quality of life as well as the economy all around the world. The World Bank estimated that 40% of the world's population will face the scarcity of water by the end of 2030, which is predicted to challenge one-fourth of the world economy. Additionally, flooding will result in the loss of billions of dollars as well as cause life threats (World Bank, 2017). This will pose an adverse environmental effect leading to threats to human life, food security, and energy production (Hirpa et al., 2019). Therefore, water resources should be managed properly to minimize the various environmental impact that can occur in the future (Joshi et al., 2020a; Rahaman et al., 2019). However, the sustainable management of water resources is being difficult due to natural drivers such as climate change and anthropogenic factors such as population growth and urbanization (Chattopadhyay & Jha, 2016; Middlekoop et al., 2001; Duran-Encalada et al., 2017)

Climate change is an alarming topic that is posing many extreme hydrological events such as floods, heatwaves, and droughts, all over the world. The International Panel on Climate Change (IPCC) projected an increase of 1.5- 2 degrees centigrade of temperature between 2030 to 2052 (Allen et al., 2018). Rising temperature could lead to the changes in hydrological cycles (Griffin et al., 2013;Joshi et al., 2020c Nyaupane et al., 2018a), along with changing precipitation which could eventually impact the variability of streamflow (Bhandari et al., 2020; Basheer et al., 2016; Koirala et al., 2014; Anjum et al., 2019). Also, due to anthropogenic factors

such as urbanization, impervious area is increasing day by day causing several flash floods (Joshi et al., 2019a; Maheshwari et al., 2016, Shrestha et al. 2020a).

One of the hydroclimatic variables, streamflow, also known as channel discharge, can be used to predict long-term change (Hirabayashi et al., 2008; Chen et al., 2018). Streamflow quantity is considered critical, as it can cause disastrous flooding when flow is high, on the other hand whereas the water ecosystem can be affected severely with decreasing flow. Since streamflow is interconnected with the weather parameters such as air temperature, precipitation, and relative humidity, climate change can have an adverse effect on streamflow with the alteration of these parameters (Bhandari et al., 2020). Both high and low flow effects i.e., floods and droughts, are likely to occur more frequently across the globe with increased intensity (Roy et al., 2001; Arnell and Gosling, 2016). These increases in both high and low flow extremes have already occurred in some parts of the world and are making societal infrastructure more sensitive to climate change (Easterling et al., 2000). Moreover, extreme events are becoming more frequent and are anticipated to continue at the same frequency or even faster in the future. Such an increase in frequent extreme events drives researchers toward analyzing the hydrological component and its forecasting methods.

Many researchers have emphasized the use of different climate models, considering different hydro-climatic variables, to evaluate the future streamflow and its impact (Qi et al., 2009; Neff et al., 2000; Li et al., 2007; Mukundan et al., 2019). For the evaluation of future streamflow, different climate agencies are continuously working to provide future climate projections that can give more accurate estimation of future weather conditions. However, the uncertainties involved with the climate model are hard to remove. Consequently, multi-model ensemble method and bias-correction techniques are introduced to remove or minimize model

biases (Eyring et al., 2016). In this study, bias-corrected multimodel ensemble streamflow projection was utilized which were then routed in the hydraulic modeling software HEC-RAS to generate floodplain inundation maps. With the help of floodplain inundation maps, hazard, vulnerability, and risk assessments were performed to understand the severity of flooding and its impact on different land use.

1.2 Problem Statement and Objectives

Flooding is one of the most frequently occurring natural hazards in the world, along with droughts and heatwaves (Stefanidis & Stathis., 2013; O'Cornor & Costa., 2003, Nyaupane et al., 2018c). Due to the changing intensity and frequency of extreme rainfall, different parts of the world are facing deadly flood events causing a significant loss of life and property (De Paola et al., 2018). Some studies (Alfieri et al., 2015; Arnell, 1999) analyze the potential impact of climate change and flood risk on a global scale, where they discuss the change in flood frequency and its impact on the populated area in different parts of the world. In the United States, various studies (Bhandari et al., 2020; Chattopadhyay & Jha, 2016; Johnson et al., 2015) evaluated the change in regional streamflow due to the changes in climate. Arnell et al. (1999) showed that the alterations in annual precipitation distribution in North Carolina with the warming climate might increase extreme flooding events and water quality problems in the future. Moreover, global warming is a threat for a coastal state like North Carolina. As per the IPCC, rising sea levels due to global climate change pose a high risk for coastal communities and low-lying areas, as there will be a higher possibility of consequences such as high tides, storms, and flooding. Johnson et al. (2015) predicted, under different future climate change scenarios, that the Neuse River Basin (NRB) in North Carolina will experience an increase in streamflow due to increases in rainfall intensity. In recent years, NRB has endured deadly flood hazards due

to heavy rainfall from tropical storms and hurricanes (Ana in 2015, Matthew in 2016 and Florence in 2018). Hall (2019) estimated annual losses of $54 billion across the United States due to extreme flooding events induced by tropical storms and hurricane.

The objective of the current study is to forecast the future design discharge and floodplain inundation extent to assess the future flood risk imposed upon the Neuse River in North Carolina. The novelty of the study is forecasting the extent of the floodplain and assessment of the risk of flooding using future and historical streamflow projections made available through Coupled Model Intercomparison Project Phase 6 (CMIP6). This study also compared the future and existing Federal Emergency Management Agency (FEMA) flooding scenarios with the calculated future design discharge to understand the increased severity of flooding in future years. Two design discharges, a 100-year return period and a 500-year return period were used in the one dimensional (1D) hydraulic modeling simulation using HEC-RAS to produce flood inundation maps. Moreover, this study evaluates the difference in the extent of historic flooding with projected future flooding under a changing global climate. Hazard assessment and vulnerability assessment were employed to analyze the anticipated flood risk and help shed light on the severity of risk within the study area. Finally, the risk zone mapping was performed using the projected design discharges. In so doing, this study forecasted the future floodplain inundation area. It also assessed the future flood risk to determine the extent of flood-affected urban and agricultural areas due to increasing streamflow. The outcome of this study will enable policymakers to employ better water resources management measures and lower the risk under the future climate.

Research Question #1: What would be the impact of climate change on future streamflow, and how will it affect the flood frequency for Neuse River, North Carolina?

Assumption #1: The impact of climate change is explicitly depicted, with the use of CMIP6 streamflow projection.

Hypothesis #1: With the change in climate, frequency, and magnitude of peak streamflow is increasing in Neuse River, North Carolina.

Research Question #2: Under the projected design streamflow, what would be the future change in flood extent and patterns?

Assumption #2: Different climate models depict the future change in flood characteristics mainly, the flood extent.

Hypothesis #2: The Neuse River floodplain inundation area is increasing with the change in climate in the Kinston City

1.3 Approach

In this study, the impact of CMIP6 climate models on streamflow projection is analyzed in the Neuse River, NC near the city of Kinston. Four different future scenarios i.e. SSP1-2.6, SSP2-4.5, SSP3-7.0, and SSP5-8.5, are selected from the eight different future scenarios, along with the historical scenario where each of the scenarios includes at least two Global climate models (GCMs). Historical scenario ranges from 1950-2014 and future scenarios are extended from 2036-2100, where both the scenario share the same length of timeframe i.e. 65 years' period. The annual peak streamflow obtain from the bias-corrected data of multimodel ensemble climatic projection scenarios are utilized for the prediction of future peak streamflow, that is routed in HEC-RAS for the hydraulic modeling. Based on the inundation maps and flood patterns obtain, the impact of climate change on the streamflow can be analyzed. Further, the inundation map is utilized for the flood risk analysis which would provide the future consequences of variability in streamflow.

1.4 Thesis Organization

This thesis is composed of seven chapters. Chapter one encompasses the background of the study including the problem of statement and objective of the study. Also, it briefly describes the different approach used in this research. Further thesis organization is discussed in chapter one. Chapter two describes the literature review part where the previous research is reviewed and are correlated with the importance of current research. Also, the impact of climate change in the hydro-climatic variables is discussed in this chapter. Chapter three present the study area where the research is focused on. Also, this chapter further gives information on different types of data that are used in the study. The methods employed in this research work are discussed in chapter four. In chapter five, the prediction of streamflow, model calibration, inundation mapping, and flood risk assessment are presented. Also, the discussion of various uncertainties associated with the study is included in the same chapter. The conclusion and limitations associated with this research are concluded in chapter six. To extend this research for future researchers, the recommendation was provided in chapter seven. Lastly, the references and the appendices followed the chapters.

CHAPTER 2

LITERATURE REVIEW

2.1 Introduction

According to the 2018 IPCC report, climate change is causing different extreme hydrological events that are having impacts on the hydrological cycle and human livelihoods all over the world (Allen et al., 2018). Also, climate change plays a vital role in the ecosystem shift, leading to an increase in global warming (Merz et al., 2014; Easterling et al., 2000; Joshi & Dongol., 2018; Joshi et al.,2020d). Moreover, greenhouse gas (GHG) emissions, induced by anthropogenic factors, are escalating the rate of global warming. If the rate of GHG emissions continues to increase at the same rate as today, global warming is predicted to increase from 1.5 to 2 °C by 2052 (Allen et al., 2018). The rising trend in global warming maximizes the evaporation rate of surface water and soil moisture that will affect the amount of precipitation all around the globe (Griffin et al., 2013; Ford et al., 2018). This type of alteration in the hydrologic cycle will affect the runoff and availability of both the surface and subsurface water, which eventually impacts river streamflow (Middlekoop et al., 2001). Furthermore, the regional precipitation trend will be affected by the patterns of ocean currents and wind, which will ultimately result in a change in streamflow. So, different literature suggested analyzing the effect of climate change in the hydroclimatic variables for the proper management of water resources (Joshi et al., 2020b; Ngigi et al., 2009; Kalra et al., 2013).

Various studies showed the importance of different climatic simulations and improved hydrologic/hydraulic simulation to analyze the effect of climate change in streamflow (Bai et al., 2019; Nyaupane et al., 2018a; Thakali et al., 2016). Kalra et al. (2008) suggested the use of hydro-climatological data for the historical scenario for the estimation of future scenarios. In the

past studies, many researchers used different hydro-climatological variable such as streamflow, soil moisture, precipitation, groundwater that involved the projection of different climate variables such as precipitation temperature and humidity to access the impact of climate change (Setegn et al., 2011; Oguntude & Abiodum, 2013; Thomas & Nigam, 2018; Joshi et al., 2020b; Kalra et al., 2017). The variability in a climatic variable can have a great impact on water resource management, so the analysis should be performed considering the change in the climate.

To assess the impact of climate change on hydro-climatological variables (i.e. precipitation, temperature, streamflow), CMIP was started in 1995 under the World Climate Research Program. CMIP is a skeleton for performing the comparison of GCMs using an atmospheric model coupled to the dynamic ocean, a simple land surface, and thermodynamic sea ice. It helps to study climate change from past to future in the multimodel context with the change in radioactive forcing and natural, unforced variability (Eyring et al., 2016; Meehl et al., 2014).

The sixth phase of CMIP, CMIP6, is focused on the intercomparison of different climate models and provides the result to the user community, especially to IPCC sixth assessment report working groups. In the fifth phase of CMIP, CMIP5, climate projection was primarily based on the GHG emission, land use, and air pollutant representing representative concentration pathways (RCPs). However, CMIP6 climate projections were driven by scenarios based on SSP which is also an updated and revised version of RCPs (Riahi et al., 2017). In CMIP6, ScenarioMIP is a primary activity that provides climate model projection which is based on the different alternative scenarios that are related to the mitigation of climate change, adaption, and impact (O'Neil et al., 2016). ScenarioMIP is based on the multi-model climate projection, where

the new scenarios were that guided by new emission and land use scenario that represent the integrated assessment models (Riahi et al., 2017). Some literature suggested that the multimodel experimental design was of a dire need to build a scientific framework for understanding the climate systems as well as the change in climate, which highly influences the design of CMIP6 that includes anthropogenic drivers such as future emission, land use along with socioeconomic developments (Stouffer et al., 2017; O'Neil et al., 2016). Also, in various literature, historical and future scenarios that are made available by CMIP6 were utilized to evaluate the impact of climate change. (Shrestha et al., 2020b; Chen et al., 2020; Cook et al., 2020)

GCMs are the primary tools for the simulation of the climate change projection in the future. It provides the resources to understand potential changes in regional and global climates (Joshi et al., 2020b; Moradkhani et al., 2010; Alfieri et al., 2017). Different studies have suggested the use of climate projection from various GCMs to understand the variability of a different climatic variable in the future (Gosling & Arnell, 2016; Diallo et al., 2012; Bosshard et al., 2014; Kendon et al., 2010; Khalyani et al., 2016; Reshmidevi et al., 2018). So, the GCMs outputs are the most efficient approach that can be used for the evaluation of the impact posed by climate change (Wilby & Harris, 2006). Past studies have suggested the use of two or more climate projection GCMs, rather than using one GCM, since using one GCM can misinterpret the analysis (Camici et al., 2014; Prudhomme et al., 2002). Since the GCMs were large scale climate projection data with coarse resolution, they were recommended to regionalized for the given study area (Bao et al., 2019; Gao et al. ,2016; Thakali et al., 2018).

GCMs climate projections encompass different systematic error and uncertainty factors within it, well known as bias (Christensen et al., 2008; Wang and Chen, 2014; Salvi et al., 2011). Several pieces of the literature suggested correcting the model biases present in the GCMs

climate projection to avoid over or under-estimated outputs that could provide misleading information in the study (Cannon et al., 2015; Mishra et al., 2020; Zhai et al., 2020; Gupta et al., 2020; Gao et al., 2019). Different researchers used different bias correction techniques to reduce the model biases (Li et al., 2010; Michelangeli et al., 2009; Pierce et al., 2015; Yuan et al., 2016; Yang et al., 2018; Okkan & Kirdemir et al., 2016).

Different GCMs were utilized by numerous studies (Kay et al., 2009; Roy et al., 2001; Arnell et al., 2016) to discuss the various climate change simulation considering the extreme daily precipitation. However, there are limited studies (Nyaupane et al., 2018a; Ali et al., 2018; Yuan et al., 2016; Hoan et al., 2020) related to the future projection of streamflow. Some studies analyzed the GCMs climate projection for different scenarios provided in the different phases of CMIP i.e. CMIP3 and CMIP5 (Perez et al., 2014; Hirabiyashi et al., 2008). Various studies have used the precipitation, temperature streamflow projected from GCMs for the quantification of future extremes (Nyaupane et al., 2018a; Thakali et al., 2016). Probability distributions such as GEV, Log-Pearson III, Gumbel were used in past studies to predict the extremes of hydroclimatic variables (Hamza et al., 2019; Teegavarapu & Pathak 2019; Ayuketang & Joseph, 2016). Some studies used Delta Change Method (DCM) based on the Delta Change Factor (DCF) employing the historic peak to predict future extremes (Camici et al., 2014; Ruiter, 2012; Hay et al., 2000). The quantified extremes such as peak flows can be routed in the hydraulic and hydrologic models to generate flood inundation maps (Nyaupane et al., 2018a).

In past studies, hydraulic modeling was performed using HEC-RAS to route the peak streamflow to analyze the different flooding events (Alaghmand et al., 2012; Pinos et al., 2019; Cook and Marwade, 2009; Kuntiyawichai et al., 2020). Many studies generated the floodplain inundation maps and analyzed different flood characteristics for the projected climate using

RAS-Mapper (Yonehara & Kawasaki, 2020; Batchabani et al., 2016; Selvanathan et al., 2018; Karamouz et al., 2015). Also, the result of HEC-RAS simulation can be used for floodplain inundation mapping, management, and insurance studies. Some researchers extended the study up to the hazard, vulnerability, and risk assessment of floodplain using geographic information systems concluding it as an important step for flood risk management (Bathi & Das, 2016; Tingsanchil & Karim, 2005).

2.2 Climate Change

Climate is the weather condition of a certain region of the earth for a long period. Climate change can be defined as the shift of weather patterns in large scale due to the rising temperature caused by the human since the industrial age. Both the natural and anthropogenic activities are responsible for the change in climate (Bjurström & Polk, 2011; Wilby et al., 2004; National Research Council, 1983; Kalra & Ahmad, 2009; Thakur et al., 2020a; Thakur et al.,2020b; Tamaddun et al., 2017). The anthropogenic activities were noticed from the onset of the industrial revolution that has been intensifying the greenhouse effect resulting in global warming (Wilby et al., 2004). It has been leading to an increase in temperature, with the alteration of the hydrological cycle resulting in the change in extreme events (López-Ballesteros et al., 2020; Qi et al., 2009; Kelly et al., 2016).

2.3 Climate Projection

From the starting of 21st century, climate change has been a critical issue as the earth is warming up each day. So, different climate projection was introduced by different climatic model institutes, which consists of various hydroclimatic variables that are useful to access the impact of climate change in the future (Bai et al., 2019). Various research communities are

working continuously to provide more realistic models with minimum uncertainty factors so that the future scenario obtained from different climate projections can be more accurate.

2.3.1 GCMs for Climate Projection

GCM is a type of climate model that represents climate in a mathematical way utilizing the general circulation of the ocean or atmosphere. GCMs are used for the analysis of climate change and forecasting of weather integrating the different components of the earth i.e. land surface, atmosphere, and sea ice (Block et al., 2009). The increasing emission of GHG resulting the global warming is predicted with the utilization of different climatic projections of GCMs (Easterling et al., 2000). GCMs uses different emission scenario as their model output to understand the effect of climate change in the future.

2.3.2 Climate Scenarios

Different phase of CMIP coordinates with the present to future climate design and distribution to understand the impact of climate change that are anticipated in the near to far future or long period. In the fourth and fifth IPCC assessment reports, CMIP3 and CMIP5 models were developed respectively, including various GCMs (Solomon et al., 2007; Wilby et al., 2004; Bjurström & Polk, 2011). However, according to Stouffer et al. 2015, the quantification of radioactive forcing was distinguished from other external forcing factors such as GHG, in the CMIP5 scenarios that had proven it to be superior to the previous phase of CMIP i.e. CMIP3. Further, IPCC updated the forcing levels that were represented by RCPs in CMIP5 by combining it with SSPs to make it more robust in CMIP6. Figure 1 shows the detailed picture of scenario formation in CMIP6 through the integration of climate forcing level and SSPs, where SSP2-4.5 was given as an example scenario.

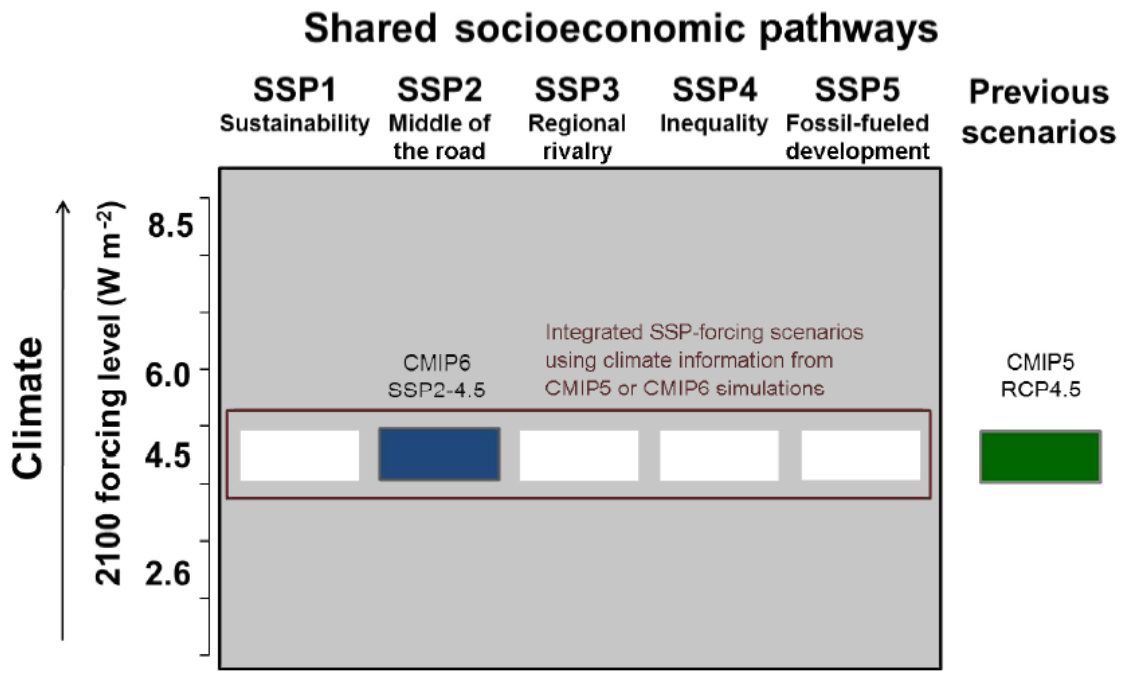

Figure 1: Illustrative figure showing the scenario formation in CMIP6

Source: O'Neil et al. 2016

The scenarios in CMIP6 shared the matrix of SSP and RCP so that it can better answer the question of earth forcing components and its responses (Riahi et al, Eyring et al. 2016). These scenarios will help in quantifying the impact of climate change and its uncertainties. Table 2 present the detailed description of tier 1 scenarios in CMIP6 that was abstracted from (O'Neil et al. 2016). Table 1 provides information on climate forcing levels and pathways of given scenarios.

Table 1: Scenarios in CMIP6 with their forcing level and SSPs

Scenario Name	Forcing Category	SSP	2100 Forcing (W/m^2)
SSP1-2.6	Low	1	2.6
SSP2-4.5	Medium	2	4.5
SSP3-7.0	High	3	7.0
SSP5-8.0	High	5	8.5

2.3.3 Bias Correction of GCMs

The Climate projection of various GCMs consists of model biases that need to be rectified. Various bias correction techniques were adopted by different studies to rectify the model biases (Pierce et al., 2015; Wilby et al., 2004, Shrestha et al., 2020c). Statistical and dynamic downscaling are the two different approaches for bias correction of large-scale climate projection GCMs. In the statistical approach, the relationship between the GCMs and local climate data is developed. It depends more on the historical data and involves less computation that makes it easier to implement and interpret as well (Wilby et al., 1998 & 2004; Huang et al., 2011). For the statistically meaningful and stable relation between historic and future scenarios, Huang et al. (2011) suggested the use of the time series of at least 30 years for the bias correction.

CDF-t is one of the statistical methods of bias correction that can be useful for analyzing the uncertainty in the various hydroclimatic variable (Vrac et al., 2016; Famien et al., 2018; Yuan et al., 2012; Guo et al., 2020). CDF-t was developed by Michelangeli as the extension of quantile matching which provides and deals with CDFs. It assumes the translation of CDF of GCMs variables is only possible where the transformation function exists (Michelangeli et al.,

2009). Many studies (Pierce et al., 2015; Guo et al. 2018) have concluded the use of CDF-t as an effective bias correction method as it reduced or rectified biases from large-scale climatic data. So, this study also used CDF-t to minimize the biases of CMIP6 based streamflow data before the hydraulic simulation.

2.4 Flood Frequency Analysis

To evaluate the peak discharge, the flow was calculated for different year return period interval. Different probability distributions were utilized in past studies, where GEV was found to be a more efficient and better fit for the streamflow and other hydroclimatic variable distributions (Hamzah et al., 2019; Nyaupane et al., 2018a). So, GEV was recommended as a statistical best fit distribution to predict future extremes (Kalra et al., 2020b), especially for hydroclimatic variables (Santos et al., 2016; Kasiviswanathan et al., 2017). GEV is a parametric distribution, which utilizes shape, location, and scale parameters to find the cumulative probability for the given event (Hosking et al., 1985). Previous study by Hosking and Wallis (2005) suggested L-moment as one of the methods that were widely used for the estimation of the three parameters used in this distribution. GEV was previously used in the streamflow distribution of the humid subtropical regions (Re & Barros, 2009; Santos et al., 2016). It can be employed for the estimation of design flows at different recurrence intervals.

For the prediction of future peak flows, the DCM can be used. DCM utilizes the historic and future peak flows to get DCF. The DCF as the ratio of future and historic flow need to be further utilized with the existing scenarios to get design flow for the future designed scenario. Past studies have suggested DCM as one of the effective ways to predict future extremes (Hay et al., 2000; Nyaupane et al., 2018a). The equation involved in DCM for the future flow estimation is given below:

$$\text{DCF} = \frac{\text{Future Design Flows}}{\text{Historical design Flows}} \quad (1)$$

$$\text{Peak future design year flow} = \text{DCF} * \text{Existing design year flows} \quad (2)$$

According to FEMA, the design year for the flood analysis can be taken as 2,5,10,25,50,100 and 500 years. The Flood Insurance Report (FIS) generated by FEMA considers 100-year peak flow as the design peak flow (FIS, 2013).

2.5 HEC-RAS Model

HEC-RAS, a hydraulic analysis program, was developed by the US Army Corps of Engineers in 1995 to work in a network that would support multi-user and multi-tasking environments. HEC-RAS helps to simulate water surface profiles for steady and unsteady flow, water quality analysis, and sediment transport computation, utilizing a graphical User Interface for interaction with the system (Brunner, 2016; Joshi et al., 2019a; Kalra et al., 2020a). The model can perform both 1D and two-dimensional simulation. It requires digital elevation models cross-section, land use, and slope of terrain to simulate the model.

1D modeling can be done for both the steady and unsteady flow of the river. Many researchers have applied the HEC-RAS 1D steady analysis for the simulation of a floodplain flows and to understand the characteristics of the flood (Yang et al., 2006; Lim, 2011; ShahiriParsa et al., 2016; Mehta et al., 2013; Peng & Liu, 2020). Further, the FEMA recommended the use of the HEC-RAS steady model for the modeling and remodeling of different streamflow to make the FIS more effective (FEMA, 2018). The 1D steady model used the steady discharge data at the upstream cross-section of the reach as input data to calculate the water surface profile (Ahamad et al., 2016; Kumar et al., 2017; Kalra et al., 2020b). Other inputs such as geometric, land use, and elevation data were also employed in the study. For the defined cross-sections, water surface elevation levels (WSEL) are the main output along with the flood

extent, channel velocity, and top width. During the simulation, the conservation of energy was applied from cross-section to cross-section throughout the length of the stream channel (Brunner, 2016). Also, the streamflow discharge is constant over time in the stream.

Additionally, using the RAS Mapper, HEC-RAS can generate inundation maps and analyze flood patterns. The outcome of HEC-RAS simulation can be used for floodplain inundation mapping, risk assessment, management, and insurance studies (Mihu-Pintilie et al., 2019; Tingsanchil & Karim., 2010).

2.6 Floodplains Inundation Mapping and Risk Assessment

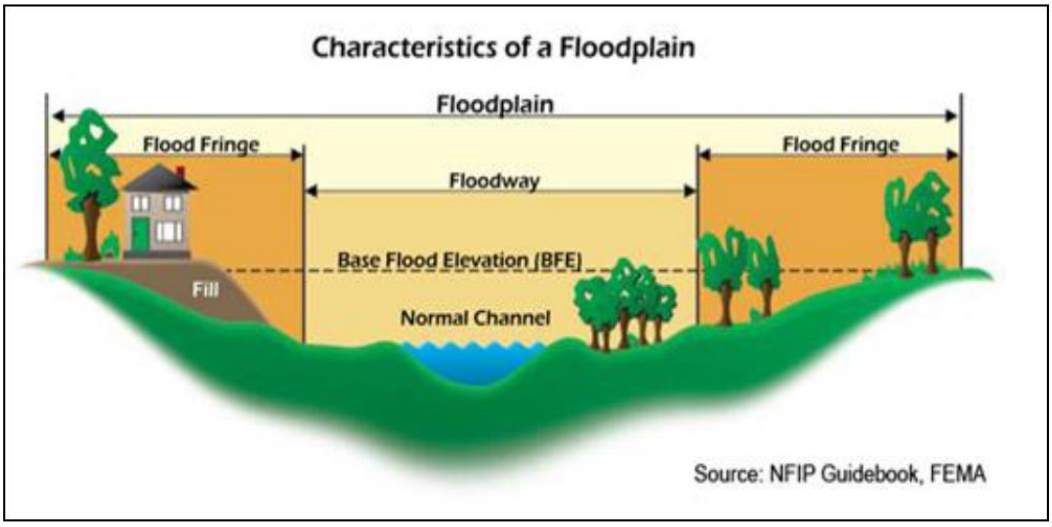

Figure 2: Description of Cross-section in the main channel

Source: NFIP Guidebook (2009), FEMA

Floodplains are the land area adjacent to the river or streams that extend from the bank of the river to the valley edges that experience flooding when discharge gets high. Floodplain consists of two parts i.e. floodway and flood fringe. The floodway is the main channel whereas the flood fringe is the outer bank of the river extending to the valley. Figure 2 gives a detailed picture of the characteristics of floodplains.

When the river/stream experience high discharge, then it can cause risk to human life and the infrastructure located in the floodplains, which can result in loss of life and property. FEMA has classified the floodplains into different zones based on the severity of the risk. Also, FEMA administered the NFIP to provide insurance in case of flooding hazards. NFIP also encourages the regulation of flood management at the community level to mitigate the effects of flooding in inundated areas (FEMA, 2018 & 2019)

Tingsanchali and Karim (2010) deduced that the impact of future flooding could be identified using a hazard, vulnerability, and risk assessment to mitigate human losses and attenuate economic as well as environmental losses. Thus, flood hazards, vulnerability, and risk assessments provide a framework for the management of flood risk. Furthermore, Noren et al. (2016) suggested that a risk assessment is a vital step in effective flood risk management for sustainable livelihood and agricultural system management. The risk zone maps can be used as source information to prepare emergency response plans, flood management and prevention programs, and infrastructure design. This study provides risk analysis and mapping to improve early responses to future floods.

CHAPTER 3

STUDY AREA AND DATA

3.1 Study Area

The study area was selected in a reach of Neuse River that originates from the confluence Eno and Flat River at Durham County, NC. The Neuse River flows toward the southeast United States in between the piedmont and Pamlico Sound ("Neuse River", 2019; "NEUSE: River of Peace", 2019). The study reach is 32 km long and extends from a latitude and longitude of 35.23° N, 77.77° W at the river's upstream with an elevation of 10.73 m to latitude and longitude of 35.25° N, 77.58° W at the river's downstream with an elevation of 4.15 m. The United States geological survey (USGS) gauge station at Neuse River, Kinston (Station ID 02089500) is located 1.2 km upstream from the downstream end of the study reach at the elevation of 3.3 m above NGVD29. The agricultural land, residential area, and wetlands dominate the study reach. The city of Kinston is the principal city within the study area, as shown in Figure 3a,b. This city has experienced numerous flooding events in the past due to extreme rainfall. The study area is a humid subtropical climate with the highest temperature in July and maximum rainfall in September with the average annual precipitation of 1235.96 mm ("US Climate Data", 2019).

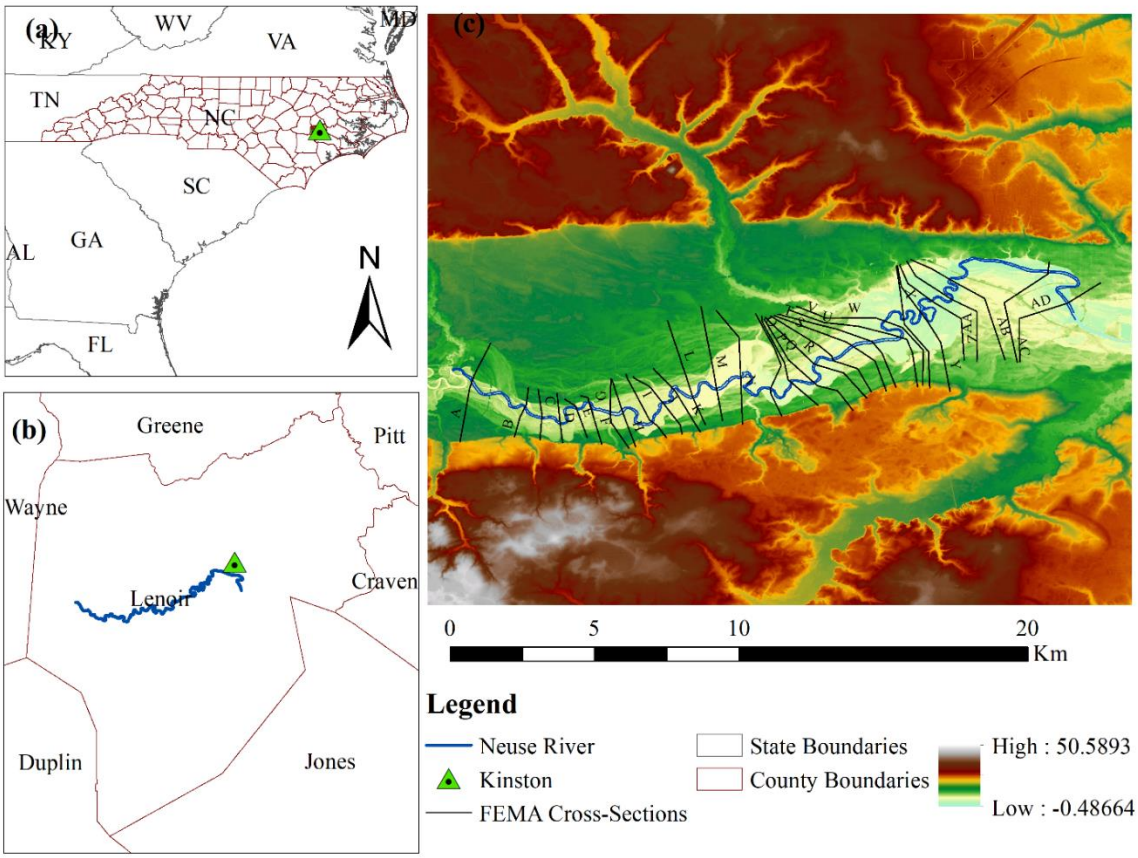

Figure 3: (a) States boundaries outlining counties of NC including Kinston City, (b) Lenoir county showing the Kinston City at downstream of the study reach, (c) existing information of the study area from a FEMA FIS report cross-sections and their labels along with their elevation.

In the past, this region suffered many extreme flood events due to many disastrous tropical storms, and hurricanes causing heavy rainfall with abrupt increase in streamflow of rivers. The tropical storm causing heavy rainfall cause threat to the people living in both the coastal area and far away from shoreline. Ione, Hazel, Donna, Fran, Floyd, and Matthews were some of the hurricanes and tropical storm that cause disastrous flooding with loss of lives and property in different part of North Carolina. In 2015, tropical storm Ana made 175 mm rainfall near Kinston resulting the freshwater flooding in Kinston and nearby area (NWS, 2020). Recently, in 2018 hurricane Florence made a devastating impact in the city of Kinston due to the

flooding resulted from the storm surge in Pamlico sound causing significant inundation in Neuse River along with landfall in a different area of NC (Stewart & Berg, 2019). The Table 2 presents major flood events caused by the hurricanes in the Neuse River along with the abrupt increase in streamflow of the Neuse River and number of fatalities in the United States.

Table 2: Major Hurricanes that cause flooding in the Neuse River and its fatalities inside the US

S.N.	Hurricane	Date	Discharge (m^3/s)	Fatalities in the US
1	Donna	08/05/1960	342.63	8
2	Fran	17/09/1996	761.72	22
3	Floyd	23/09/1999	1013.74	57
4	Mathew	10/15/2016	1061.88	28
5	Florence	09/23/2018	863.66	43

**The data are obtained from the USGS gage station 02089500 in Neuse River at City of Kinston.*

The selected reach, Neuse River, along with the city of Kinston, is located in Lenoir County, NC, as shown in Figure 3b. This study used the existing information of the study area from a FEMA FIS report, hereafter referred to as FFR within this article (FIS, 2013). Figure 3c shows the digital elevation map (DEM) with the elevation information of the study reach along with the FFR assigned cross-sections.

3.2 Input Data

Using a single GCM can have more uncertainties in the results (Camici et al. 2014), so this study utilized scenarios of CMIP6 consisting of two or more GCMs. Specifically, this study used four scenarios among twelve available scenarios. Eight scenarios were eliminated due to having only one GCM, and daily streamflow data from selected scenarios were used to evaluate

the peak streamflow of the study reach. In CMIP6 Atmosphere-Ocean General Circulation Models, three GCMs for the historic year were available with several climatic projections which were obtained from the model institute named Centre National de Recherches Meteorologiques/Centre Europeen de Recherche et Formation Avancees en Calcul Scientifique (CNRM-CERFACS). A long modeling period from 1950 to 2014 is taken as a historic period. For future streamflow datasets, four different scenarios i.e., SSP1-2.6, SSP2-4.5, SSP3-7.0, and SSP5-8.5, each having two different GCMs from 2036 to 2100 were utilized to access the impact of a hydroclimatic variable in the future. These four different future scenarios include climate-changing anthropogenic factors, along with the socio-economic developments (O'Neil et al., 2016). Table 3 presents the scenarios used in this research along with the number of ensemble members.

Table 3: GCMs climate projection for historical and future scenarios used in the study along with the number of ensemble members and modeling institute.

Scenarios	Model Name			Modeling Institute
	CNRM-CM6	CNRM-ESM2	CNRM-CM6-HR	
Historical	√ (24)	√ (5)	√ (1)	CNRM-CFRFACS
SSP5-8.5	√ (5)	√ (6)		CNRM-CFRFACS
SSP3-7.0	√ (5)	√ (6)		CNRM-CFRFACS
SSP2-4.5	√ (5)	√ (6)		CNRM-CFRFACS
SSP1-2.6	√ (5)	√ (6)		CNRM-CFRFACS

**Source: DOE, 2019*

The historical observation data were extracted from the USGS gauge station 02089500 near the Neuse River of NC. The gage station is located downstream of the selected reach so that

it can be used for the calibration and validation of the HEC-RAS 1D model. The data were selected from 1950 to 2014. The gridded streamflow data from CMIP6 has centroid near this USGS gauge station.

The USGS national map viewer provides the DEM (https://viewer.nationalmap.gov/basic/). For a model with higher accuracy, the literature suggested finer resolution DEM (Saksena & Merwade, 2015; Peng & Liu., 2019). However, due to the limitation of available data, this study used 10-m resolution DEM. Figure 3 shows the DEM of the study reach showing the elevation along with the FFR assigned cross-sections. The land use and land cover data were obtained from the website of Multi-Resolution Land Characteristics Consortium (MRLC) provided the land use and land cover data, which provides the Manning's roughness coefficient of different land use (MRLC, 2016). In this study, the most recent National Land Cover Dataset (NLCD) 2016 data were used. Table 4 present the various land cover along with the Manning's coefficient assigned for the land type by NLCD, 2016.

Table 4: Land Use and Land Cover 2016 with assigned Manning's Coefficient

S.N.	Name	Manning's value (n)
1	no data	
2	barren land rock/sand/clay	0.04
3	cultivated crops	0.06
4	deciduous forest	0.1
5	developed high intensity	0.15
6	developed low intensity	0.1
7	developed medium intensity	0.08
8	developed open space	0.04
9	emergent herbaceous wetlands	0.08
10	evergreen forest	0.12
11	grassland/herbaceous	0.045
12	mixed forest	0.08
13	open water	0.035
14	pasture/hay	0.06
15	shrub/scrub	0.08
16	woody wetlands	0.12

The location of the river cross-sections was selected in and between the cross-section assigned by FFR to aid in the calibration of the hydraulic model. Since the detail of structures like dams, the levee location elevations were not readily available, they were not considered in this study. Furthermore, Manning's values were adopted from FFR for the selected reach length of the Neuse River. FEMA developed a hydraulic analysis flood along with the prediction of

different year recurrence flows. Since FEMA performs the flood frequency analysis based on a 100-year and 500-year return period, this study followed the same course, i.e., 100-year (0.1% chance) and 500-year (0.2% chance) of annual occurrence of flooding events. Table 5 shows the extreme streamflow discharges obtained from FFR near Kinston City, NC for the Neuse River.

Table 5: Summary of discharge (m3/s) at USGS gage site 02089500, downstream of study reach given by FFR.

Flooding Source	Location	Drainage Area (Sq. Km)	10% Annual Chance (m^3/s)	2% Annual Chance (m^3/s)	1% Annual Chance (m^3/s)	0.2% Annual Chance (m^3/s)
Neuse River	Approximately 1.2 km upstream of the confluence of Adkin branch	6972.25	639.96	982.59	1146.83	1574.42

CHAPTER 4

METHODOLOGY

The methods section is divided into two sub-sections. First, it explains the statistical analysis to predict future design discharge. Secondly, it depicts a detailed guideline of hydraulic analysis to generate the flood inundation maps and further assessment of potential hazard, vulnerability, and risk. Figure 4 presents the steps involved in this study as the flowchart, which are further discussed below in a sequential manner.

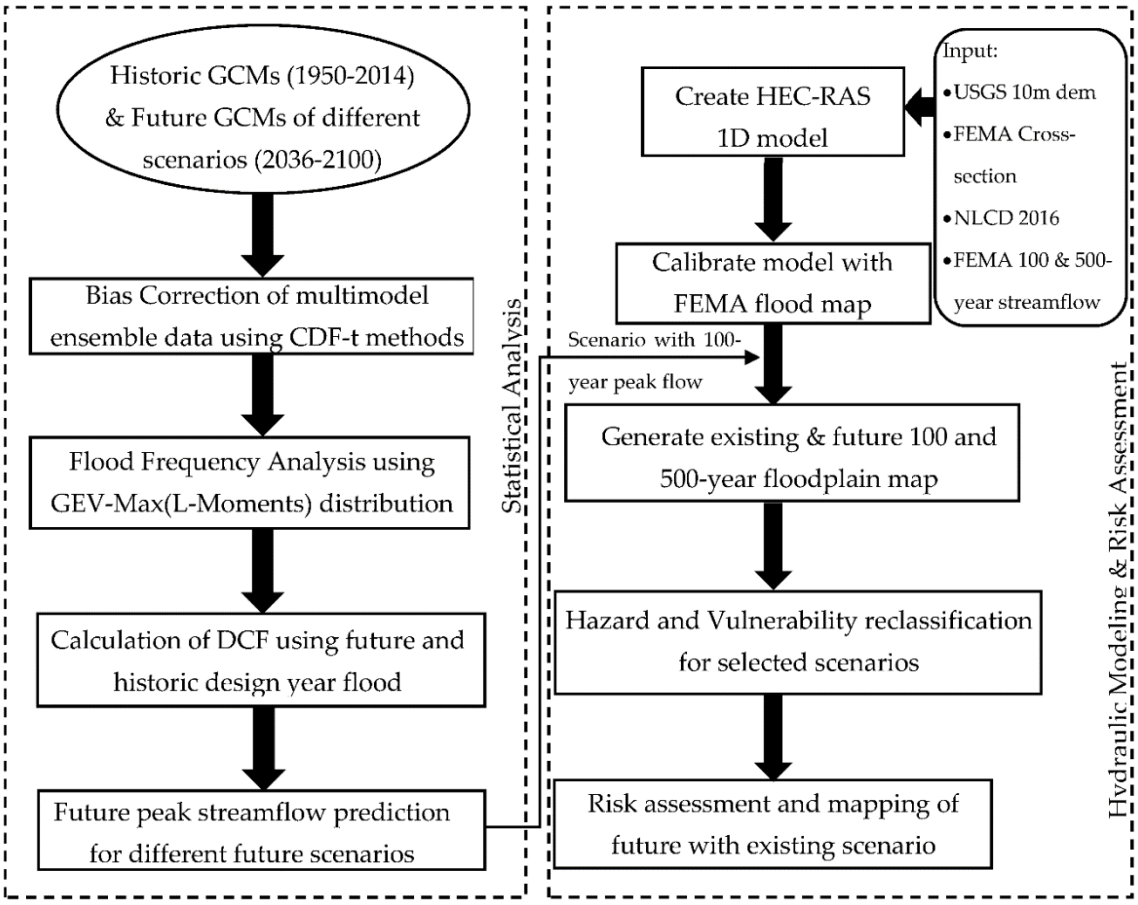

Figure 4: Schematic diagram showing the sequential steps followed to analyze flood frequency, predict the future streamflow, flow routing, floodplain mapping, and risk assessment.

4.1 Statistical Analysis

The following two sub-subsections discuss the statistical analysis involves bias correction of CMIP6 streamflow data and quantification of the future design flows.

4.1.1 Bias Correction

The streamflow data obtained from CMIP6 consist of significant systematic biases, that requires bias correction before further application. Moreover, before bias correction, an ensemble of GCMs was performed for each of the scenarios, so that it would increase the robustness in predicting future change (Shrestha et al., 2020b; Nohara et al., 2006; Sillmann et al., 2013). In this study, the CDF-t method was chosen for the bias correction of multimodel ensemble CMIP6 streamflow data (Guo et al., 2018; Pierce et al., 2015). The CDF-t method develops the relationship between modeled and observed CDF outputs, considering the transformation function "T", where daily observed data were utilized (Michelangeli et al., 2009).

The descriptive figure to describe the CDF-t methods is as shown in Figure 5, where the modeled future (F_{gf}) and historical climate data (F_{gh}) along with historical observed historical data (F_{sh}) have been used to obtain future bias-corrected data (F_{sf}). Figure 5 shows the F_{sf} as the green dotted line. The bias-corrected value of F_{gh} should fall within the range of F_{sh}. All three arrows, a, b, and c showed the sequential steps of bias correction. Since it is impossible to plot the future change beyond the maximum F_{sh}, arrow "b" moves right toward arrow "c" to intersect the green dot line, which finally generates the bias-corrected data.

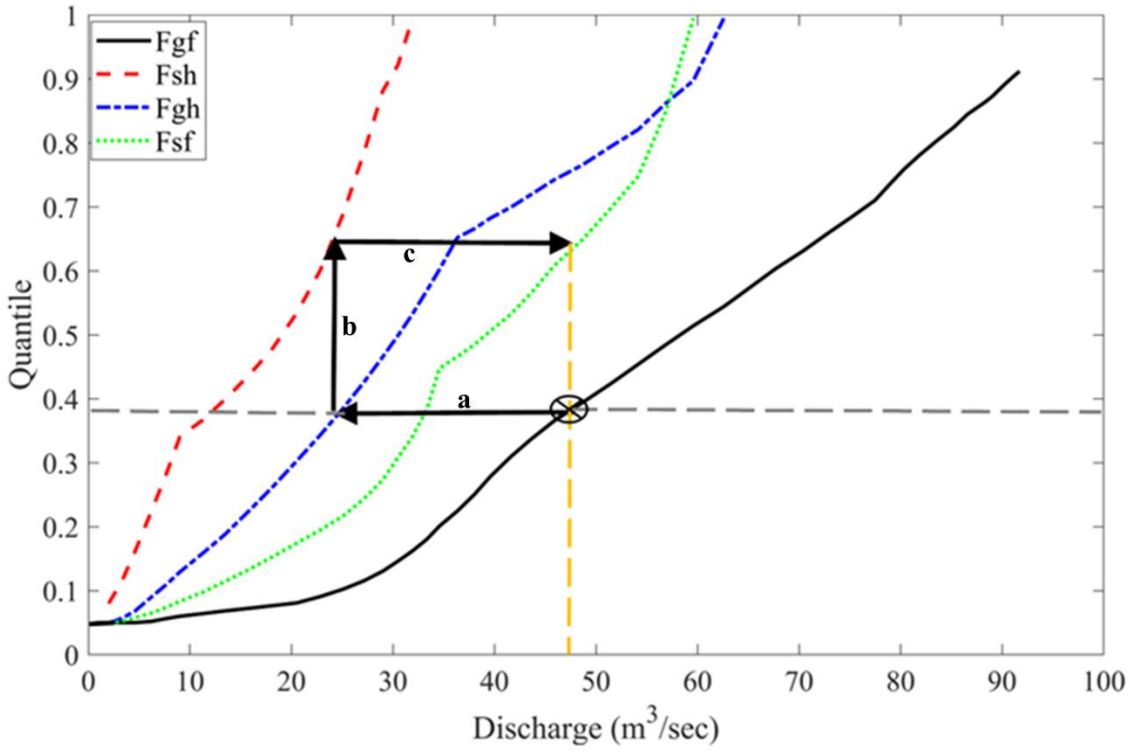

Figure 5: Illustrative figure showing bias correction using CDF-t methods.

The following develops the series of the equation used for the bias correction starting with:

$$T\left(F_{Gh}(x)\right) = F_{sh}(x) \tag{1}$$

Let us consider, $u = F_{Gh}(x)$, that gives us $x = F_{Gh}^{-1}(u)$, where $u \in [0,1]$.

Then, Equation (1) is transformed to

$$T(u) = F_{sh}\left(F_{Gh}^{-1}(u)\right) \tag{2}$$

where *T* represents the functional relationship between the modeled and observed CDF results concerning the historical period.

Validating the Equation (2), the final CDF-t equation is:

$$F_{sf}(x) = F_{sh}\left(F_{Gh}^{-1}\left(F_{Gf}(x)\right)\right) \tag{3}$$

Here, the functional relation is established between observed and modeled streamflow for historical data to be utilized for future periods. Furthermore, the utilization of modeled projection and estimating the CDF of future climate projection is performed, and hence, the bias-corrected data is used for the prediction of future flow.

4.1.2 Quantification of the Future Design Flow

After the bias correction of streamflow data, the next step is to calculate future design flow. Annual peak streamflow is extracted from each multimodel ensemble scenario (SSP5-8.5, 3-7.0, 2-4.5, 1-2.6) for future time series of 2036 to 2100. Annual peak flow is also calculated for the observed historical time series of 1950 to 2014, from the same USGS gauge station as an earlier step. Then GEV probability distribution is utilized to analyze the annual maximum flow for different recurrence intervals. The equation that was used by the GEV distribution for the annual maxima is given below.

$$\mathrm{GEV}(x:\mu,\sigma,\kappa) = \begin{matrix} exp\left\{-\left[1+\kappa\left(\frac{x-\mu}{\sigma}\right)\right]^{-1/\kappa}\right\} & if\ \kappa\neq 0 \\ exp\left\{-exp\left[-\left(\frac{x-\mu}{\sigma}\right)\right]\right\} & if\ \kappa=0 \end{matrix} \quad (4)$$

In this equation, μ, σ, and κ are GEV parameters respectively representing the location, scale, and shape of the data. Additionally, for shape parameter $\kappa > 0$, $\mu - \sigma/\kappa < x < \infty$; $\kappa = 0$, $-\infty \leq x \leq \infty$; $\kappa < 0$, $-\infty \leq x \leq \mu - \sigma/\kappa$ (Hosking et al 1985). Using L-moments, location, scale, and shape parameters are calculated to fit the GEV distribution. Thus, the obtained peak flows for different year return periods are utilized for the estimation of future peak flow. Peak flow for 100 and 500-years is calculated for both climate modeled and observed data with GEV for hydraulic analysis. After the GEV analysis, the DCM is used utilizing the ratio of future to historic peak discharge known as DCF. DCF helps to estimate different design flood events for evaluation of future peak flows (Nyaupane et al., 2018a). The main idea of using DCM is to match the currently observed gage streamflow data and FFR streamflow data. For individual scenarios (SSP5-8.5, 3-7.0, 2-4.5,

1-2.6), DCF is calculated and a scenario with higher DCF is chosen for further study. The selected scenario with higher DCF will exhibit an increase in future design flow in its maxima. Thus, GEV generated streamflow for a 100-years and 500-year return period is multiplied by the DCF to predict future design streamflow.

4.2 Hydraulic Modeling

The hydraulic modeling is performed using the 1D steady model on of HEC-RAS (version 5.0.7). Different studies have proven the HEC-RAS 1D steady model to be effective in analyzing the floodplain and hydraulic parameters (Yang et al., 2006; Lim, 2011; Mehta et al., 2013). The model used DEM, land use data, FEMA cross-sections, and different design year streamflow for the simulation to generate the floodplain inundation in the study area. The HEC-RAS model included a total of 95 cross-sections, including 30 existing from FFR to address the critical points along the reach. Manning's roughness coefficient was assigned as suggested by the FFR. The analysis uses the FFR 100-year discharge to calibrate the model with the help of the known WSEL. The WSEL was given by FFR, 2016.

The observed and simulated WSEL was used for the calibration of the simulated model. It will show the robustness of the model generated (Mehta et al., 2013; Kalra et al., 2020b). During the calibration, the FFR assigned 30 cross-sections were selected. The model performance was measured using different statistical measures such as Nash-Sutcliffe Efficiency (NSE), Root Mean Square Error (RMSE), Coefficient of Determination (R^2), and Percent-Bias (PBIAS) (Joshi et al., 2019a). The NSE, RMSE, R^2 and PBIAS were calculated utilizing the following equations:

$$NSE = 1 - \frac{\sum_{i=1}^{n}(O_i - S_i)^2}{\sum_{i=1}^{n}(O_i - O_{avg})^2} \quad (5)$$

$$RMSE = \sqrt{\frac{\sum_{i=1}^{n}(O_i - S_i)^2}{n}} \quad (6)$$

$$R^2 = \left(\frac{\sum_{i=1}^{n}(O_i - O_{avg})(S_i - S_{avg})}{\sqrt{\sum_{i=1}^{n}(O_i - O_{avg})^2}\sqrt{\sum_{i=1}^{n}(S_i - S_{avg})^2}} \right)^2 \quad (7)$$

$$PBIAS = \frac{\sum_{i=1}^{n}(O_i - S_i) * 100}{\sum_{i=1}^{n} O_i} \quad (8)$$

Where,

O_i : the observed WSEL

S_i : the simulated WSEL

O_{avg} : the average of WSEL

S_{avg} : the average WSEL

After the calibration, the model was routed for the future peak flow obtained for the "quantification of future design flow" step. In the study, four future scenarios were used to determine the peak design flows utilizing DCM. Among the four scenarios, the scenario with the maximum 100-year and 500-year design flow was selected for the generation of floodplain inundation maps. These flows were employed for both existing and future scenarios, and the floodplain inundation extent was developed in RAS-Mapper. The flood inundation area was mapped using the ArcGIS (Version 10.7.1, Environmental System Research Institute (Esri), Redlands, CA, USA) so that the hazard classification can be performed. Also, the selected future scenario was compared with the existing FEMA floodplain inundation areas so that it aids in understanding the increase of flood risk in future years.

4.3 Hazard and Risk Classification

Hazard and vulnerability assessments were considered as the vital steps in accessing the flood risk (Klijin et al., 2015). For the hazard assessment, different flood characteristics such as

water velocity, water depth, and flood extent can be considered as the indicators for hazard classification. This study used water depth for the hazard assessment and attempted to classify the water depth and distinguished the hazard of that area based on the threat posed by flooding on human life. For both extreme events, 100-year, and 500-year, four hazard categories are generated (Tingsanchali & Karim, 2005 & 2010). Hazard class was divided into a low hazard (H_1), moderate hazard (H_2), high hazard (H_3), and severe hazard (H_4) class based on the critical flood depth range from 0.8 m to 3.5 m. These hazard classes along with their description are presented in Table 3. In this study, 0.8 m was considered as the level above the ground floor level and 3.5 m was considered as the roof of a single-story building for residential. The human threat was set at the ease of wading at any flooding event.

Table 6: Flood hazard classification and its description considering water depth as an indicator of the degree of hazard.

Hazards Class	Flood Depth (m)	Flood Hazard	Description of Hazard
Low Hazard	<0.8	H_1	Poses less of a hazard to people, and on-foot evacuation can be done.
Moderate Hazard	0.8–1	H_2	On-foot evacuation will be difficult and adult evacuation will be difficult. The infant will be at a serious threat.
High Hazard	1–3.5	H_3	Hazard inside house and evacuation only possible from the roof.
Severe Hazard	>3.5	H_4	All the structures will be underwater, evacuation from the roof will also be a threat as people may be drowned there too.

The Floodplain area in the Neuse River is comprised of different land-use units, which are assigned by NLCD 2016, MRLC. Based on hazard threats on the landforms, risk analysis can be done by utilizing the vulnerability. Hence, as a part of vulnerability assessment, the landforms from NLCD 2016 were reclassified into residential, forest, agriculture, wetlands, and water bodies. The residential area was assigned a value of one (1) and water a value of five (5)

representing the flood risk which is lower in residential areas than in areas near the water bodies. Other classified areas such as forest, agricultural land, and wetland were assigned with values of 2, 3, and 4 values, respectively. Table 7 and Figure 6 shows the land use reclassification along with the assigned value. Previous studies showed that the vulnerabilities were assigned based on the projected flooding and socioeconomic conditions (Bathi & Das, 2016). This study utilizes vulnerabilities based on flood hazard impact and topography for both existing and future scenarios. Furthermore, the future scenarios are comprised of socioeconomic pathways and emission scenarios, that would better depict the threat of expanding floodplains due to climate change.

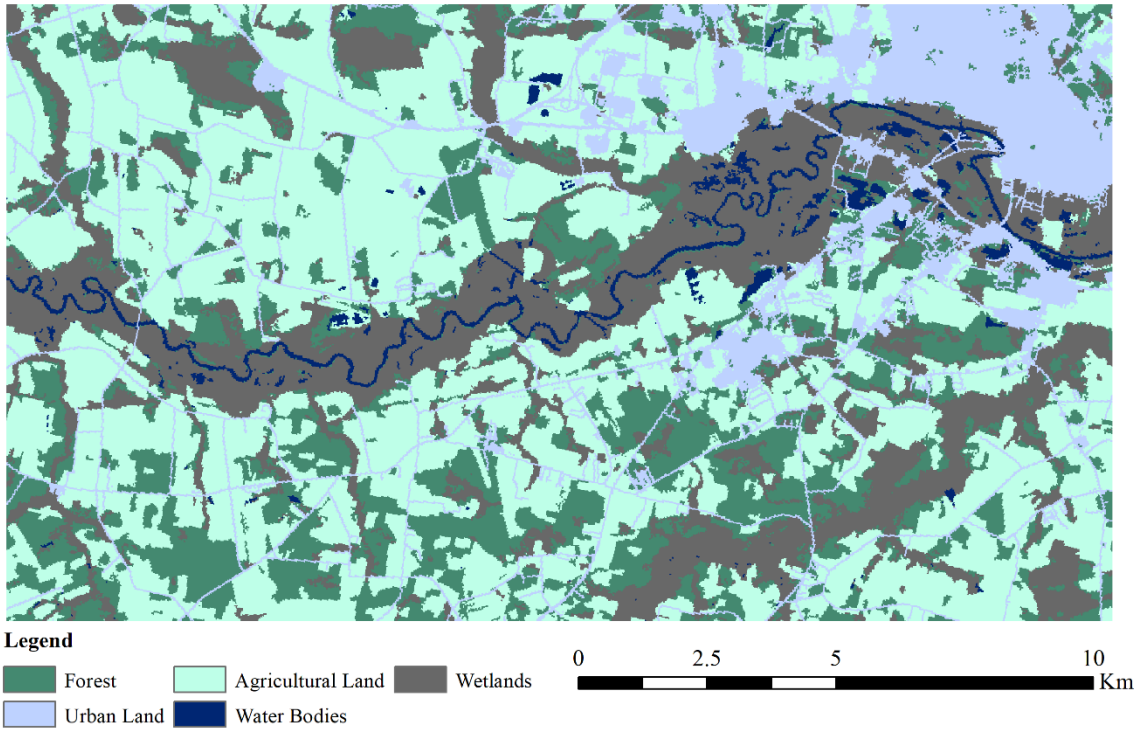

Figure 6: Reclassified NLCD map for the vulnerability assessment

Table 7: Reclassification of the land use data obtained from NLCD (2016) for the study area near Kinston with their assigned value for vulnerability assessment.

Land Classification (NLCD 2016)	Reclassification of Land Use	Score
Developed High Intensity Developed Low Intensity Developed Medium Intensity Developed Open Space	Urbanized Area	1
Deciduous Forest Evergreen Forest Mixed Forest Barren Land Grassland/Herbaceous Shrub/Scrub	Forest	2
Cultivated Crops Pasture/Hay	Agricultural Land	3
Emergent Herbaceous Wetlands Woody Wetlands	Wetlands	4
Open Water	River	5

After that, a risk assessment was performed by utilizing classified flood hazards due to flooding, which evaluates the threat posed to different landforms based on floodplain depth. Therefore, the magnitude of flood risk was reckoned as a multiplying of the flood hazard and vulnerability, which is inferred physically by assigning values on the equal interval score- a scale

from 0 to 20. Scores of less than zero are defined as risk free zones. The risk classification assigned with the interval of scores is presented in the Table 8 below.

Table 8: Zonal Classification of flood risk based on the severity

Flood Risk Zone	Score
Risk Free Zone	≤ 0
Low Risk Zone	0-5
Moderate Risk Zone	5-10
High Risk Zone	10-15
Severe Risk Zone	15-20

The classified risk zone was used to determine the severity of flood risk in different land types. The risk-map for both the 100 and 500-year design flood for future scenarios as well as the existing scenario was developed. The map portrays the risk that could happen in the future in that area. Moreover, the risk map for the existing FEMA study was compared to the risk projected in the future.

CHAPTER 5

RESULT AND DISCUSSION

The results are discussed in four ensuing sections. The first section discusses the bias correction results of GCMs obtained from CMIP6. This section also presents future flows that were calculated using bias-corrected data. The second section highlights the simulation results of calibrated hydraulic models that predict the extent of floodplain for different climate scenarios. The third section shows the evaluation of floodplain using classified hazard data. The final section presents the outcomes of risk analysis utilizing reclassified hazard and vulnerability data.

5.1 Flood Frequency Analysis and Performance of Hydraulic Modeling

This study uses daily streamflow data obtained from the climate model projection and USGS gage station, shown in subplots (a) and (b) of Figure 7. The data shows that the range of streamflow is increasing in the Neuse River. A total of 74 streamflow projections from 3 different GCMs of different historical and future climate data were used for the analysis of annual peak flow. The historical data helped to bias-correct future projections for each scenario from the multi-model ensemble GCMs. Figure 7b shows the annual peak flows extracted from the bias-corrected daily streamflow data for each future scenario (i.e., SSP5-8.5, 3-7.0, 2-4.5, 1-2.6). Since the study area is under the risk of catastrophic flooding, the maximum flows are analyzed in this study. Figure 7a,b shows the range of intense flows for future scenarios and historical data. The data in the different scenarios illustrate that the range of flow is greater for SSP3-7.0 and SSP5-8.5 since the projected GHG emissions are at a higher level for these scenarios in comparison to other scenarios.

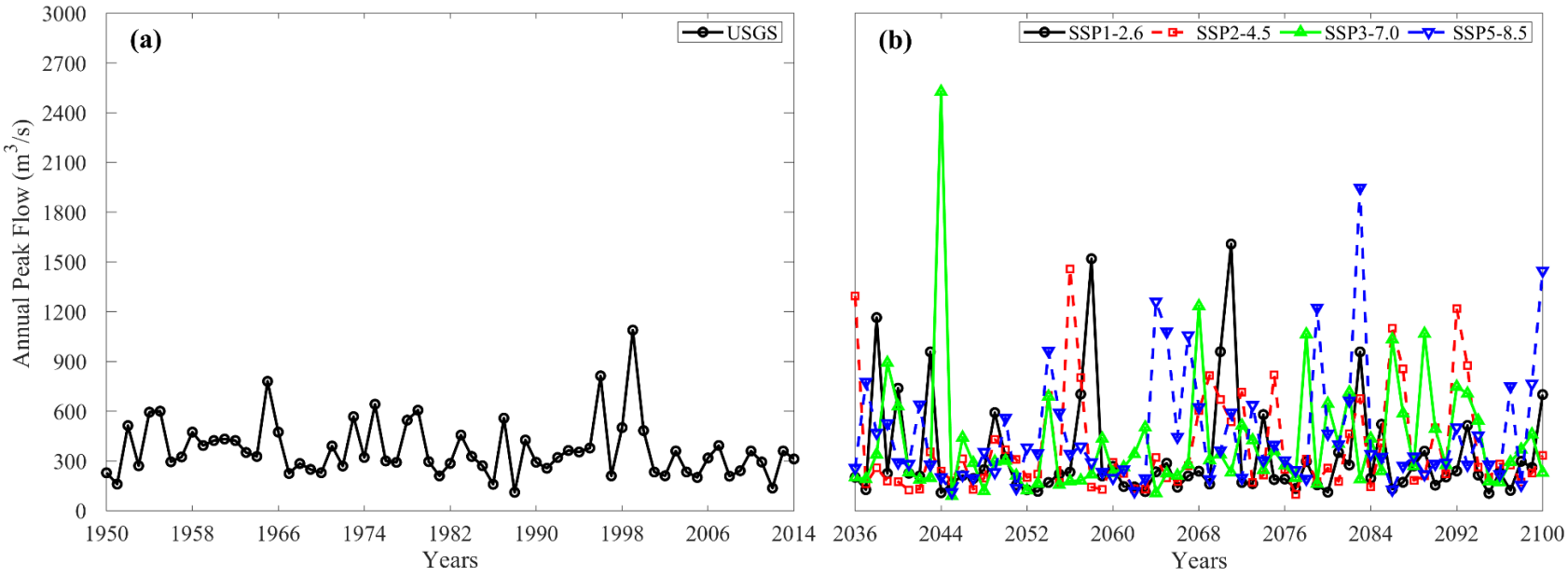

Figure 7: Annual peak streamflow for (a) historical observation data and (b) different future scenarios

For the different scenarios representing the different emission pathways, GEV-Max (L-Moments) was utilized to evaluate the design peak flows of different recurrence intervals for different future scenarios (2-year, 5-year, 10-year, 50-year, 100-year, 500-year). Considering the 100-year return period flood, the historic and future scenarios, i.e., SSP1-2.6, SSP2-4.5, SSP5-8.5 were utilized for the calculation of peak discharge, where the discharge was found to be 939.58 m^3/s, 1814.93 m^3/s, 1780.34 m^3/s, 1917.87 m^3/s, and 1921.65 m^3/s, respectively. Across all four future scenarios, SSP5-8.5 generated the maximum flows as the result of higher emission scenarios producing higher radioactive forcing (i.e., 8.5 W m^{-2}) by 2100. For the same scenarios, the 500-year design flow was 1283.11 m^3/s, 4062.07 m^3/s, 3367.09 m^3/s, 3698.73 m^3/s, and 3455.40 m^3/s, respectively.

The DCF was calculated by utilizing the different return period discharge from GEV and FFR for the Neuse River. All future return flows were divided by respective discharges according to recurrence intervals from FFR to get DCF values. Figure 8 shows the distribution of DCF for individual scenarios. From Figure 8, it is inferred that the scenario SSP1-2.6 represents the lowest DCF, i.e., less than one, with the lowest median among all the scenarios. Moreover, scenarios SSP1-2.6, SSP2-4.5, and SSP3-7.0 have DCF values lower than the high emissions scenario SSP5-8.5. The increased value of DCF with increased emission scenarios implies that higher GHG emission, land-use change, and other integrated characteristics are likely to increase the extremes of future streamflow. Also, the DCF values for 100-year and 500-year return period for all four different scenarios are presented in tabular form in Table 9. The Scenario SSP5-8.5 has a higher DCF of 2.045 and 2.69 for 100-year and 500-year design floods.

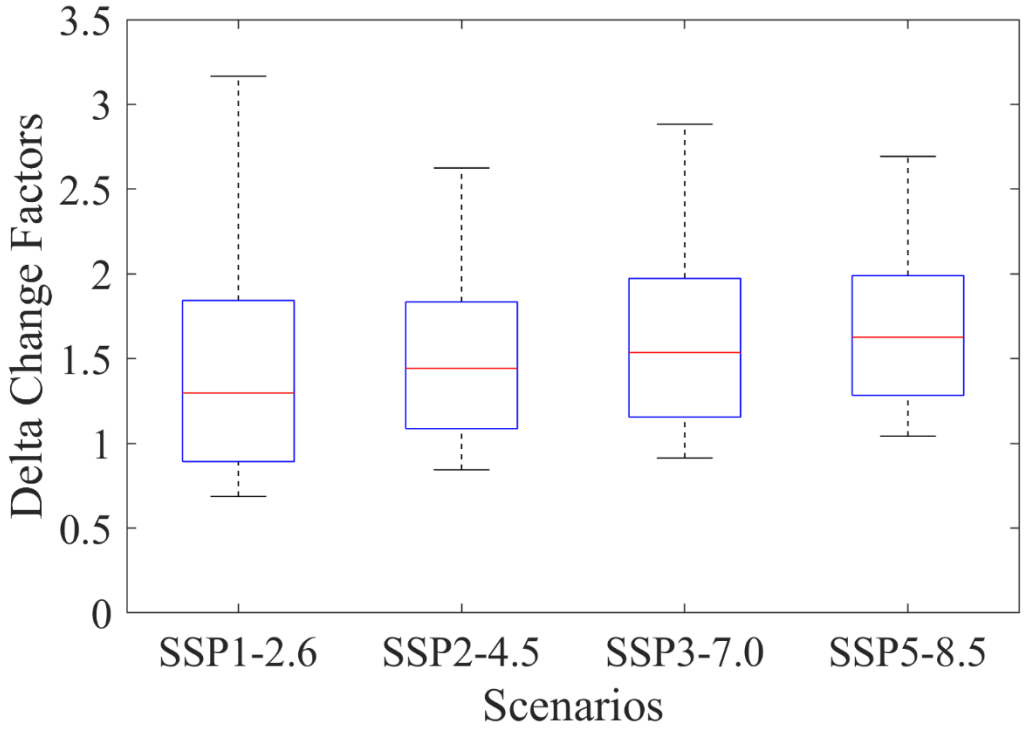

Figure 8: Box plot for the comparison of different future scenarios DCF using different recurrence intervals

Table 9: DCF values for future scenarios with 100-year and 500-year return period

Return Periods	SSP1-2.6	SSP2-4.5	SSP3-7.0	SSP5-8.5
100-years	1.931635	1.894823	2.041196	2.045215
500-years	3.165798	2.624674	2.882623	2.692987

Among all four scenarios, SSP5-8.5 based 100-year and 500-year design discharge were used to develop floodplain inundation maps. DCF value implies future design flows for 100-year and 500-year return periods at 2345.52 m3/s and 4239.88 m3/s, respectively. When comparing both the 100-year future and existing flow, the future flow is more than two times the existing flow. Similarly, in the case of a 500-year flow, future flow is nearly three times the existing flow.

The 100-year future flow even exceeds the existing 500-year flow, demonstrating the higher flood risk in the future.

The 1D hydraulic model was developed and calibrated using the FFR 100-year design flood. The comparison of observed and simulated WSEL was performed for the calibration using different statistical parameters. Furthermore, the WSEL for all 30 existing cross-sections from the FFR was used in the process. The Manning's "n" used were 0.05–0.06 and 0.12−0.19 for channel and floodplain respectively as suggested by FFR. Figure 9 shows the simulated and observed WSEL for the selected cross-sections. Statistical measures such as NSE, RMSE, $R^{2,}$ and PBIAS were used to calculate the robustness of the model by comparing the WSEL from the newly developed HEC-RAS model and FFR. The values of NSE, RMSE, $R^{2,}$ and PBIAS were 0.82, 0.40, 0.98, and −2.64, respectively, and based upon the observed and simulated data. The NSE value closer to 1 suggested that the observed and simulated WSEL were closely fitted. Additionally, the RMSE value of 0.40 shows minimal error regarding observed and simulated WSEL have a close fit. The obtained R^2 value signifies that the observed and simulated WSEL are closely matched with minimal dispersion. The negative value of PBIAS illustrates the overestimation of biases. All the calculated statistical parameters were within an acceptable range and illustrated the robustness of the calibrated hydraulic model, where the predicted WSEL can be utilized to develop a floodplain inundation map.

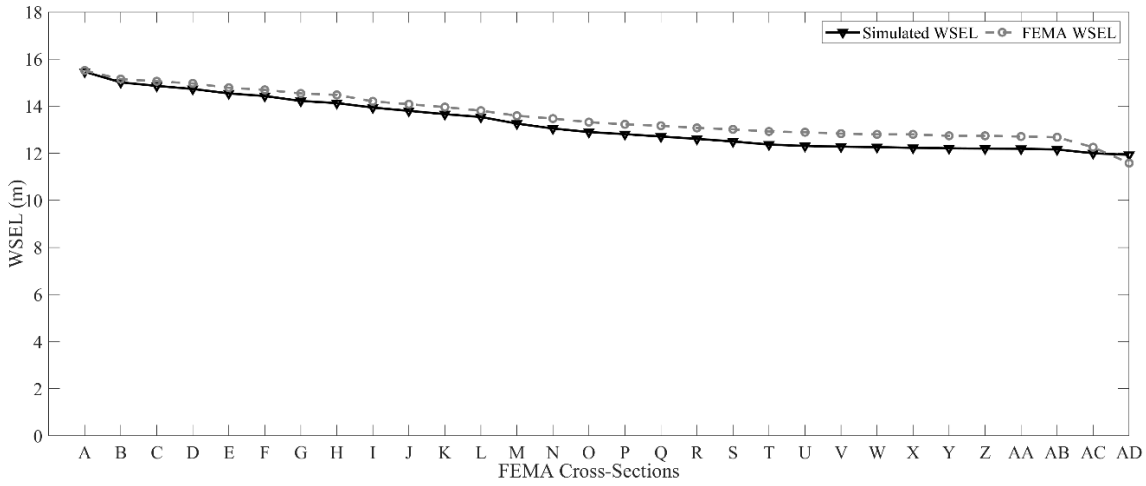

Figure 9: Calibration plot of FFR given WSEL versus Simulated WSEL

5.2 Flood Inundation Mapping

The calibrated hydraulic model was used to generate a flood inundation map. The model used DCF implied SSP5-8.5 based future design discharge for 100-year and 500-year return period. The estimated design flows are routed in the HEC-RAS model, and the floodplain inundation areas are mapped using RAS Mapper and ArcGIS. Figure 10 shows the comparison between the floodplain inundation extent generated using the existing FEMA flows and projected future flows. Both, 100-year and 500-year floodplains for future flows are much larger than existing FEMA studies. The floodplain inundation extent generated from the 100-year flood event based on future scenarios was 1.73 times higher than the FFR 100-year floodplain inundation extent. The 500-year floodplain inundation extent was 1.68 times higher than the existing 500-year floodplain extent given by FEMA. The increased floodplain inundation area due to future streamflow that might put Kinston City in a more vulnerable situation. As a coastal state, NC has plenty of low-lying areas used for agricultural purposes (Peng & Liu 2019). Those areas might be affected due to the future changing streamflow. Additionally, the selected future scenarios, SSP5-8.5, can be used in further studies to address the significant change in

streamflow linked with climate change and socio-economic change (O'Neil et al. 2016). It can make a significant difference in the field of future flood studies and emergency flood management efforts.

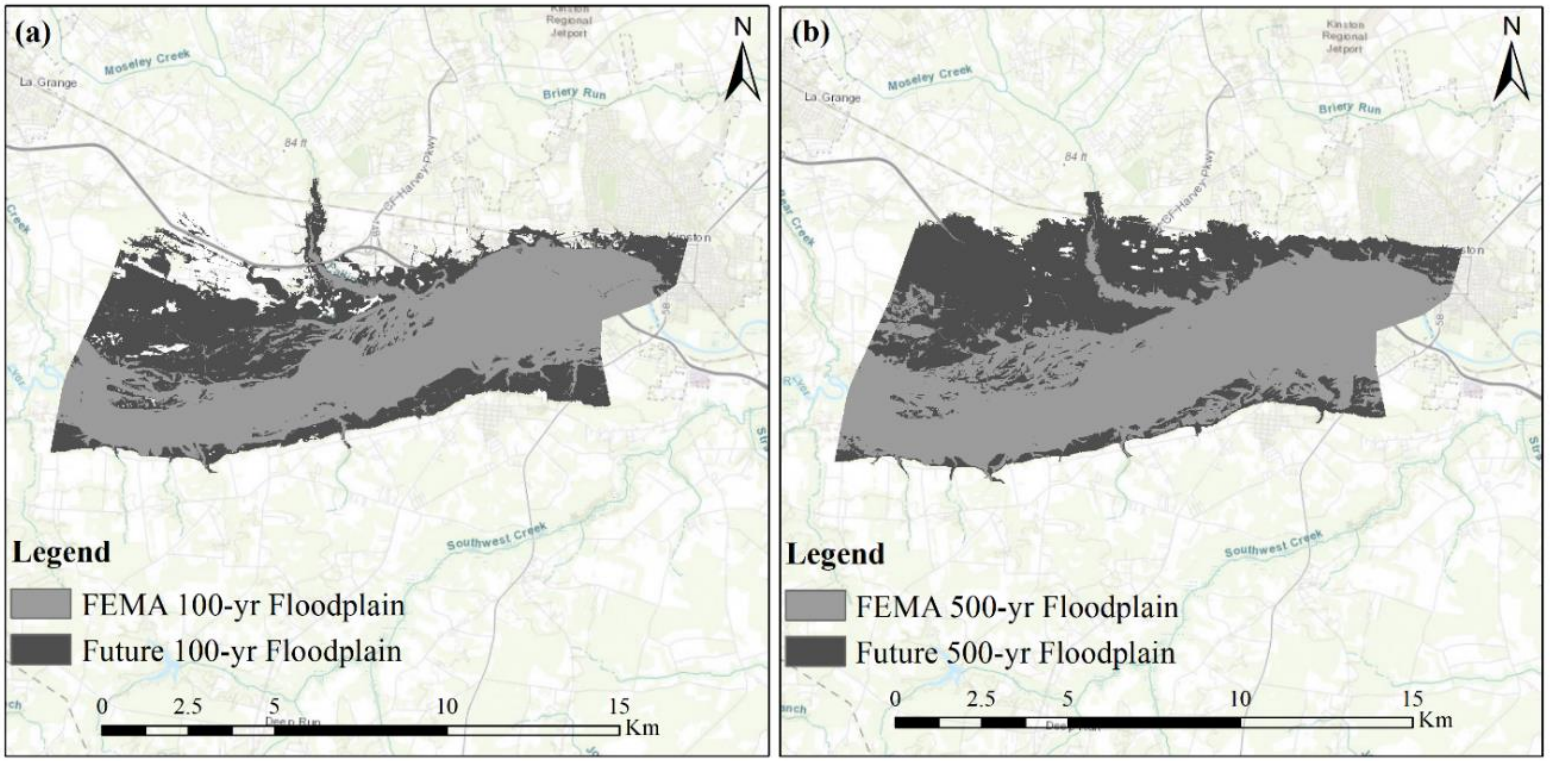

Figure 10: Comparison of flood extent map of Neuse River using the ArcMap (Version 10.7.1) between FEMA and future scenarios for (a) 100-year and (b) 500-year return period flood events, respectively.

Source: Esri, HERE, Garmin, Intermap, increment P Crop., GEBCO, USGS, FAO, NPS, NRCAN, GeoBase, IGN, Kadaster NL, Ordnance Survey, Esri Japan, METI, Esri China (Hong Kong), swisstopo, © OpenStreetMap contributors, and the GIS User Community.

Many flood characteristics were obtained as an output when performing the modeling in HEC-RAS. When generating the floodplain inundation maps for different existing and future scenarios in the Neuse River top width, channel velocity, and flood extent were exported and presented in Figure 11. Figure 11 compares all the variables (top width, channel velocity, and flood extent) for the FEMA and design discharges for the existing 30 cross-sections, acquired from the FFR, along the reach are shown in Figure 11. The projected future 100-year maximum channel velocity, computed as 1.17 m/s, is higher than the maximum channel velocity. The flood extent area for the future scenario was more than double the area for most of the cross-section in a 100-year flood and more than three times the area for the 500-year projected floodplain when compared to FEMA events.

Figure 11a shows the significant changes in the top width for the channel with cross-sections B, C, D, E, F, and G for 100-year flood events. For the 500-year flood, as shown in Figure 11b, cross-sections D, E, and M showed a significant change in top width, which implies that the flood extent is higher in that area. Previous studies (Bathi & Das, 2016; Mihu-Pintilie et al., 2019; Nyaupane et al., 2018a) projected 100-year flood events; however, due to this significant change in these flood characteristics in this study, this study was extended up to 500-year flood events. Including the 500-year flood events demonstrates the risk of future flooding and can improve hydraulic structure designs to mitigate flood risk while considering climate change.

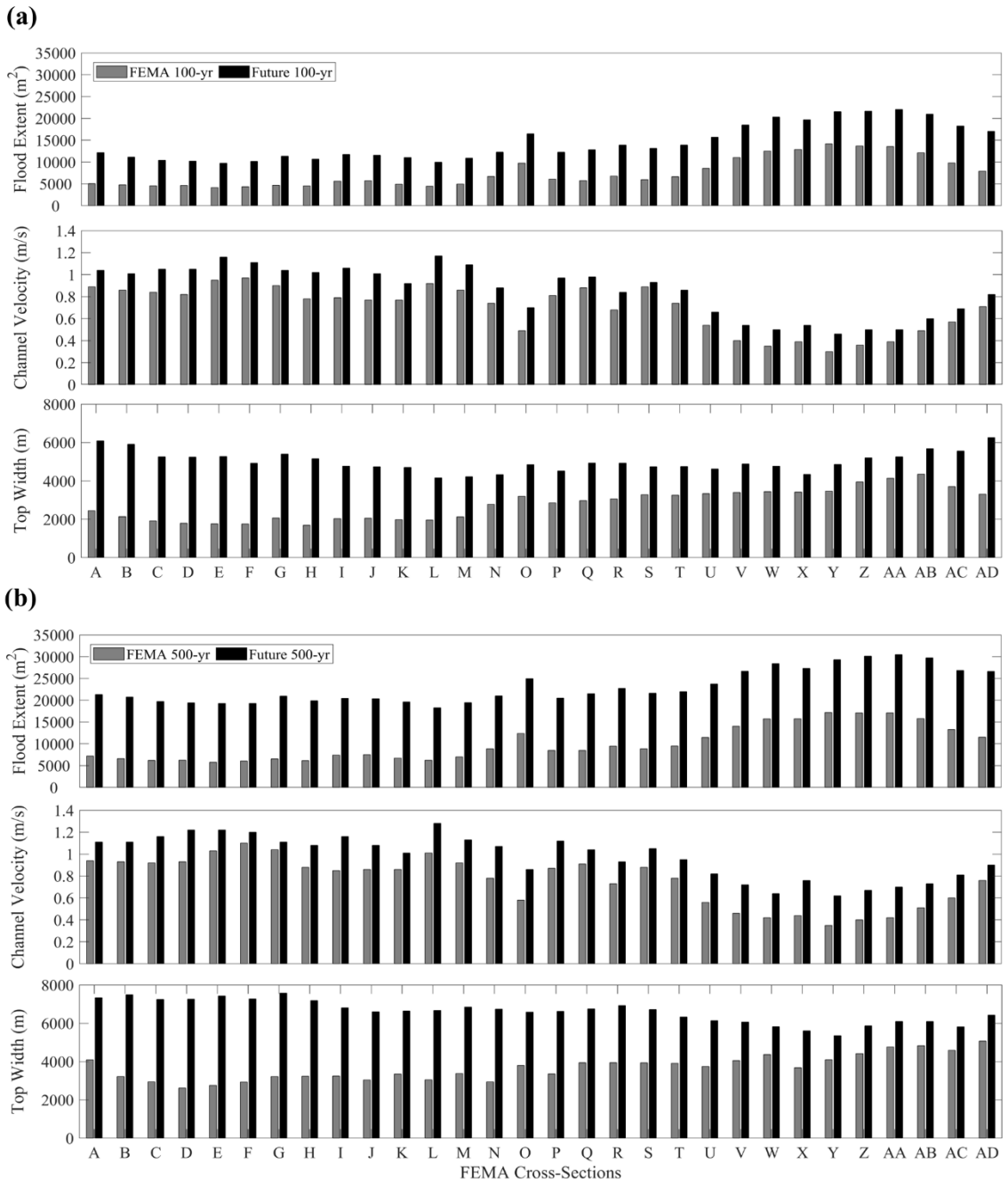

Figure 11: Comparison of flood characteristics such as flood extent, channel velocity, and top width for different flooding scenarios considering (a) 100-year and (b) 500-year return period flood events, respectively.

To assess the flood hazard, water depth was used as the quantifiable variable to study the potential threat caused due to existing FEMA and future flooding scenarios for both 100-year

and 500-year design floods. All four hazard types were classified for both existing FEMA and future flood scenarios. Table 10 outlined the flood extent covered by each hazard class for both existing and future scenarios.

Table 10: Hazard extent for the 100-year and 500-year return period flood events for both existing FEMA and future scenarios, respectively.

Hazard Class	Existing Scenario (FEMA) (km^2)		Future Scenario (SSP5-8.5) (km^2)	
	100-year	500-year	100-year	500-yr
Low Hazard	7,622.14	13,813.42	15,019.26	9,500.39
Moderate Hazard	1,457.68	2,031.19	4,667.32	2,773.16
High Hazard	16,355.02	17,497.64	27,006.62	43,377.19
Severe Hazard	19,219.03	24,634.29	30,766.75	41,845.28
Total	44,653.87	57,976.54	77,459.95	97,496.02

Also, the flood hazard mapping was performed for the existing and future scenarios so that the increase in hazard extent can be analyzed in a detailed manner in further study. Figure 12 and 13 present the extent of areas covered by each hazard classification for each scenario regarding 100-year and 500-year flood events. For the 100-year design flood, the future scenario has a higher flood hazard in comparison with the existing FEMA flooding (see Figure 12). Moreover, for this flooding event, the future scenario has a larger, severe hazard floodplain and smaller moderate hazard floodplain. For both FEMA and projected scenarios, the 100-year design flood event has a severe hazard classification with 43.04% (19,219.03 km^2) and 39.72% (30,766.75 km^2), respectively. Since the peak flow was maximum for SSP5-8.5, there could be an increase in the floodplain inundation area with possible hazard classification as low or severe.

Figure 13 shows the result from the analysis of a 500-year flood hazard assessment. It can be observed that the FEMA flood event has a lesser flood hazard extent than the future scenario (57,976.54 km^2 compared with 97,496.02 km^2) as shown in table 10. Comparing the existing flood scenario with the projected scenario for 100-year and 500-year flooding events shows the extent of hazard area increased by 1.68 to 1.73 times the existing condition, respectively. The extent of 100-year and 500-year flooding increases from existing to future scenarios, demonstrating there will be potential damage in the future. Thus, these hazard areas combine with a vulnerability factor to identify the degree of risk posed within the study area.

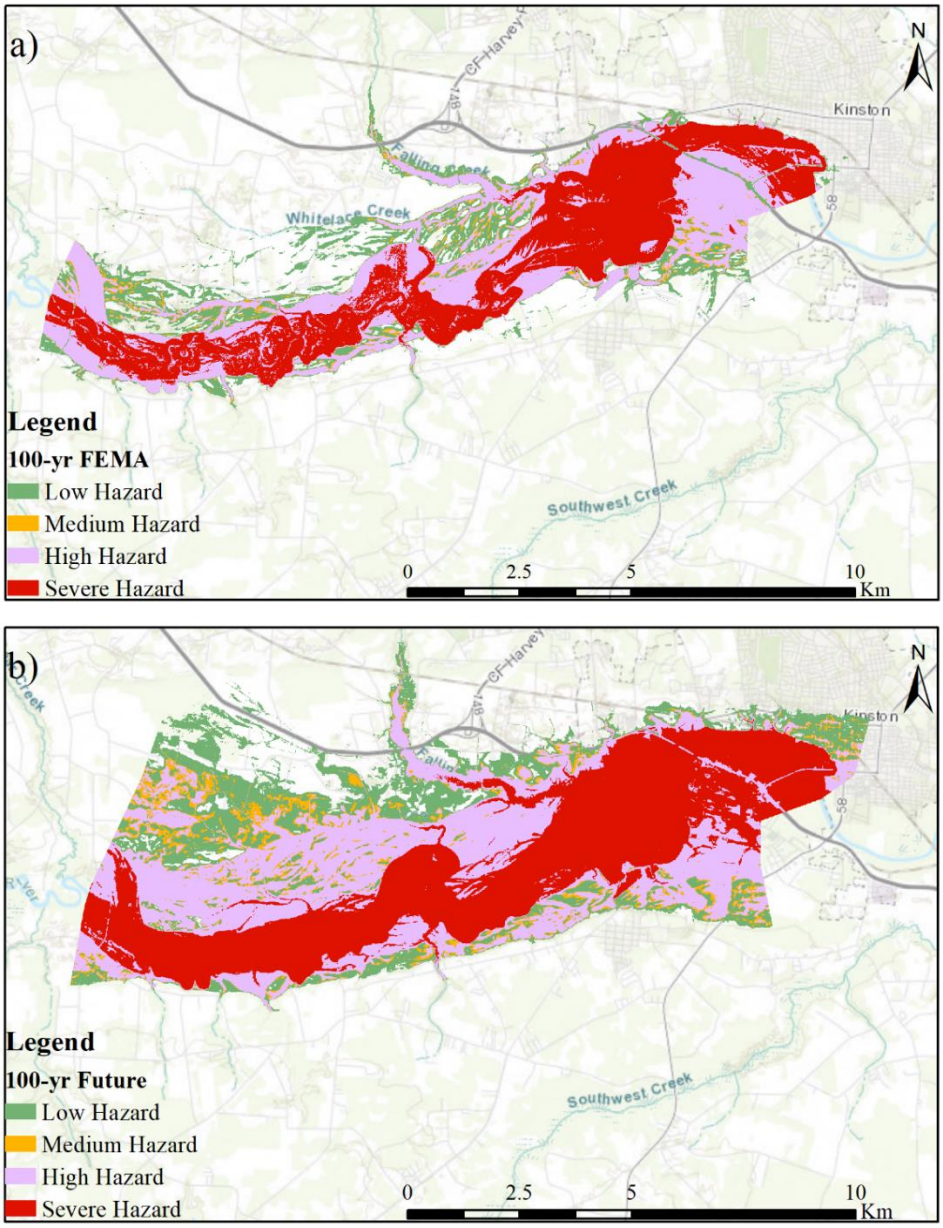

Figure 12: A Comparison of extent of flood hazard utilizing different flooding scenarios, i.e., FEMA and Future, respectively for 100 return period flood events.

Source: Esri, HERE, Garmin, Intermap, increment P Crop., GEBCO, USGS, FAO, NPS, NRCAN, GeoBase, IGN, Kadaster NL, Ordnance Survey, Esri Japan, METI, Esri China (Hong Kong), swisstopo © OpenStreetMaps contributors, and the GIS User Community.

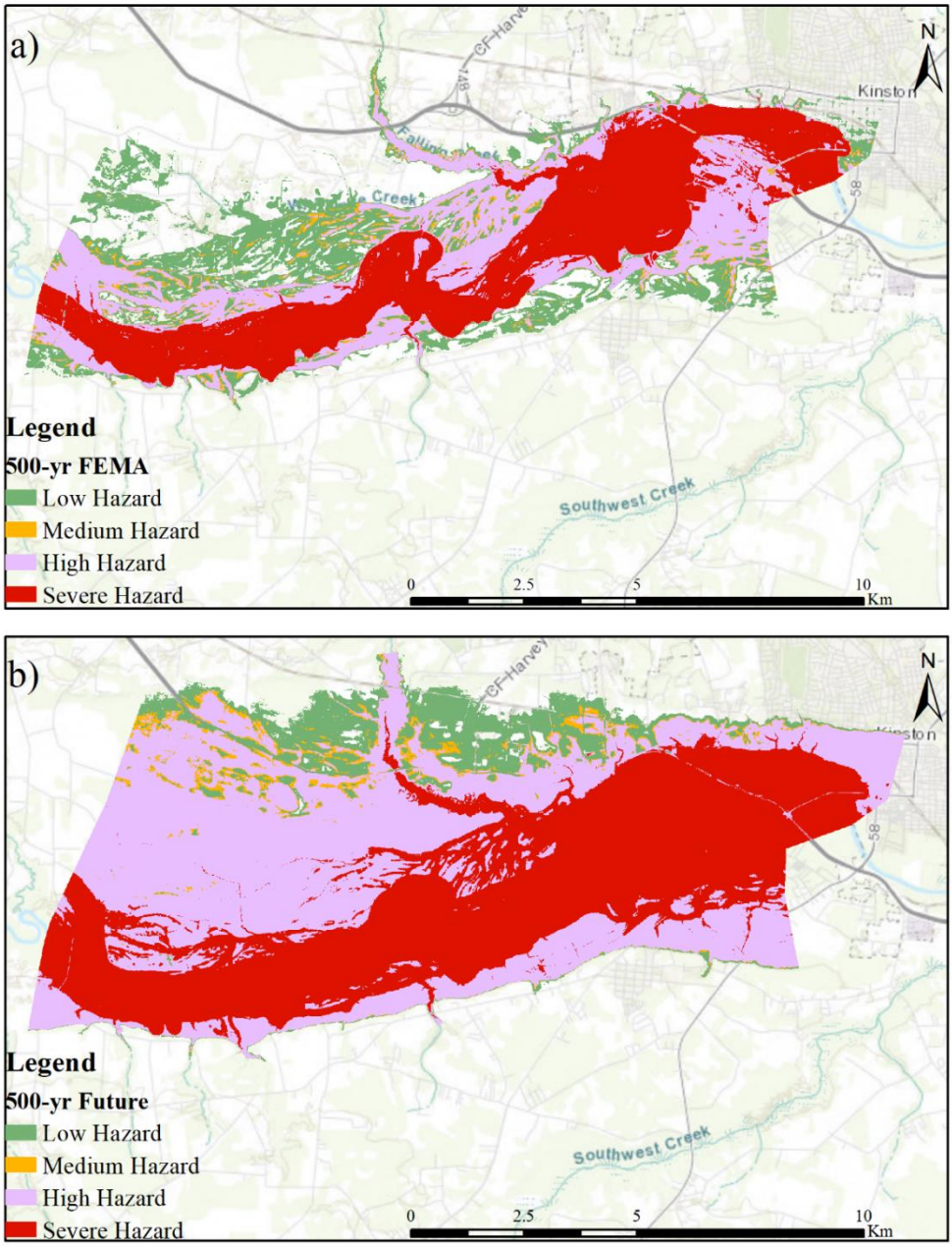

Figure 13: A Comparison of extent of flood hazard utilizing different flooding scenarios, i.e., FEMA and Future, respectively for 500-year return period flood events.

Source: Esri, HERE, Garmin, Intermap, increment P Crop., GEBCO, USGS, FAO, NPS, NRCAN, GeoBase, IGN, Kadaster NL, Ordnance Survey, Esri Japan, METI, Esri China (Hong Kong), swisstopo © OpenStreetMaps contributors, and the GIS User Community.

5.3 Risk Zone Assessment and Mapping

From the intersection of hazard and vulnerability map of FEMA and future climatic scenario SSP5-8.5, risk zone maps were extracted for 100-year and 500-year flooding events. Table 11 summarizes the area covered by each risk zone. The Risk Zone map is comprised of an area under the threat of possible damage (Alfieri et al. 2015). For the FEMA 100-year and 500-year risk maps, a greater extent of the floodplain is covered by a severe risk zone with the area coverage of 18,644.73 km^2 and 23,330.17 km^2. For the 100-year FEMA flood, a moderate risk zone has a lower area coverage among all four risk zone with an area of 6113.23 km^2. Meanwhile, in the 500-year flooding event, the flood coverage with a high risk zone has a lower area coverage with a total area of 6044.54 km^2. In the future scenario, the 500-year flood moderate risk zone covers an area of 38,869.48 km^2 or 39.75% of the total risk area. For both the future 100-year and 500-year flooding zone, the high risk zone area covered 5211.76 km^2 and 8038.58 km^2, respectively, of the floodplain area. Moreover, Table 11 shows the 100-year and 500-year FEMA flood potential risk area to be 44,659.37 km^2 and 57,979.73 km^2, respectively. Similarly, Table 11 shows the future scenario revealed a moderate risk zone for the 100-year and 500-year return periods at 77,462.86 $km^{2,}$ and 97,498.36 km^2, respectively. Additionally, it can be inferred that in contrast with the FEMA flood event, the future scenarios have a significant difference in the moderate risk zone. Furthermore, on the evaluation of 100-year and 500-year flood events, the flood risk extent of future scenarios was 1.73 and 1.68 times the existing scenarios, respectively, that shows the increasing flood risk in the future.

Table 11: Flood risk extent based on the zonal risk classification for 100-year and 500-year return period flood event for existing and future scenarios, respectively.

Risk Zone	Existing Scenario (FEMA) (km^2)		Future Scenario (SSP5-8.5) (km^2)	
	100-year	500-year	100-year	500-year
Low Risk Zone	10,468.76	18,101.99	23,773.57	21,904.91
Moderate Risk Zone	6113.23	10,503.02	22,104.30	38,869.48
High Risk Zone	9432.64	6044.54	5211.76	8038.58
Severe Risk Zone	18,644.73	23,330.17	26,373.23	28,685.39
Total	44,659.37	57,979.73	77,462.86	97,498.36

Figure 14 shows the extent of the risk zone mapped in the study area. In this study, risk zone mapping is an important factor in distinguishing the potential threat for each land use. Figure 14a shows that FEMA 100-year has a minimal threat in urbanized areas and road networks, with a larger area in the risk-free zone. The water bodies, wetlands, and forests were completely in the severe to high risk zone, which will minimize the threat to human life. Some agricultural lands are also observed to be within the low to moderate risk zone, resulting in the potential for lower crop yield during flooding events. Due to the lower elevation in the upstream side of the study area, the risk is exhibited, in contrast to the downstream part. For the 100-year future scenario (Figure 14b), the extent of all risk zone was much larger compared to the FEMA 100-year flood. For this scenario, the risk zone increased in the urbanized area and agricultural lands. Similarly, the wetlands were in a severe risk zone, whereas agricultural lands were in a low to high risk zone. More urbanized areas are located in the low risk zone, which includes

residential, industrial, and road networks, which was previously in the no risk zone for the FEMA 100-year flood event. Hence, the increase in low risk extent was higher for future scenarios, which suggests an increase in a potential threat to human settlement in the future. Due to this, there can be an increase in future streamflow that may lead to enlarged flood risk areas. It is necessary to analyze the risk for future and existing 100-year flood events since the events have a higher frequency in history and are likely to happen frequently in the future as well. Moreover, analyzing the future risk would indicate the relative change in socio-economic impact in the study area with the change in the flood hazard area.

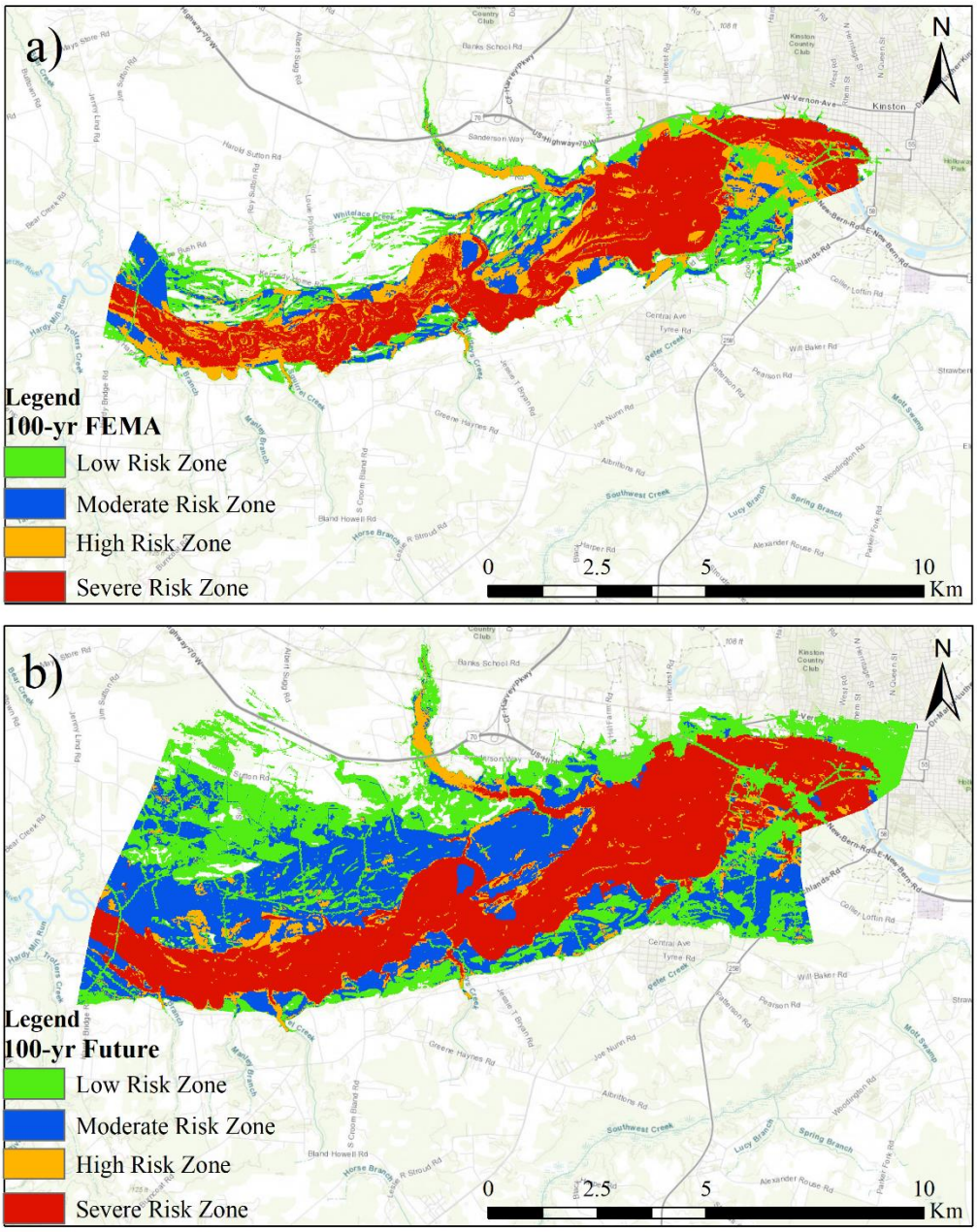

Figure 14: Comparison of extent of risk for 100-year a) existing (FEMA) and b) future scenarios utilizing the risk zonal classifications

Source: Esri, HERE, Garmin, Intermap, increment P Crop., GEBCO, USGS, FAO, NPS, NRCAN, GeoBase, IGN, Kadaster NL, Ordnance Survey, Esri Japan, METI, Esri China (Hong Kong), swisstopo © OpenStreetMaps contributors, and the GIS User Community.

The risk maps of the 500-year FEMA exhibit all classification of risk zones over the study area. The severe risk zone is larger, extending from waterbodies to the forest and some agricultural lands. The high risk zone covers some parts of the forest, agriculture, and water bodies (Figure 15a). The extent of the low risk zone was greater in an agricultural area near to upstream in the study area and lesser in urban areas, including road networks downstream. As the elevation of the city increases, the risk for the FEMA 500-year flood event decreases in the urbanized area. However, low-lying plain land used for farming purposes is under high risk. The 500-year future scenario results showed that most of the urbanized area and agricultural lands were under the low to high risk zone (Figure 15b). Figure15b also reveals the risk of flood zone with much of that land subjected to a higher risk zone. Future climate scenarios increase the risk that potential floods may have on the urbanized areas of this floodplain. Local water managers can make new development policies to mitigate this risk.

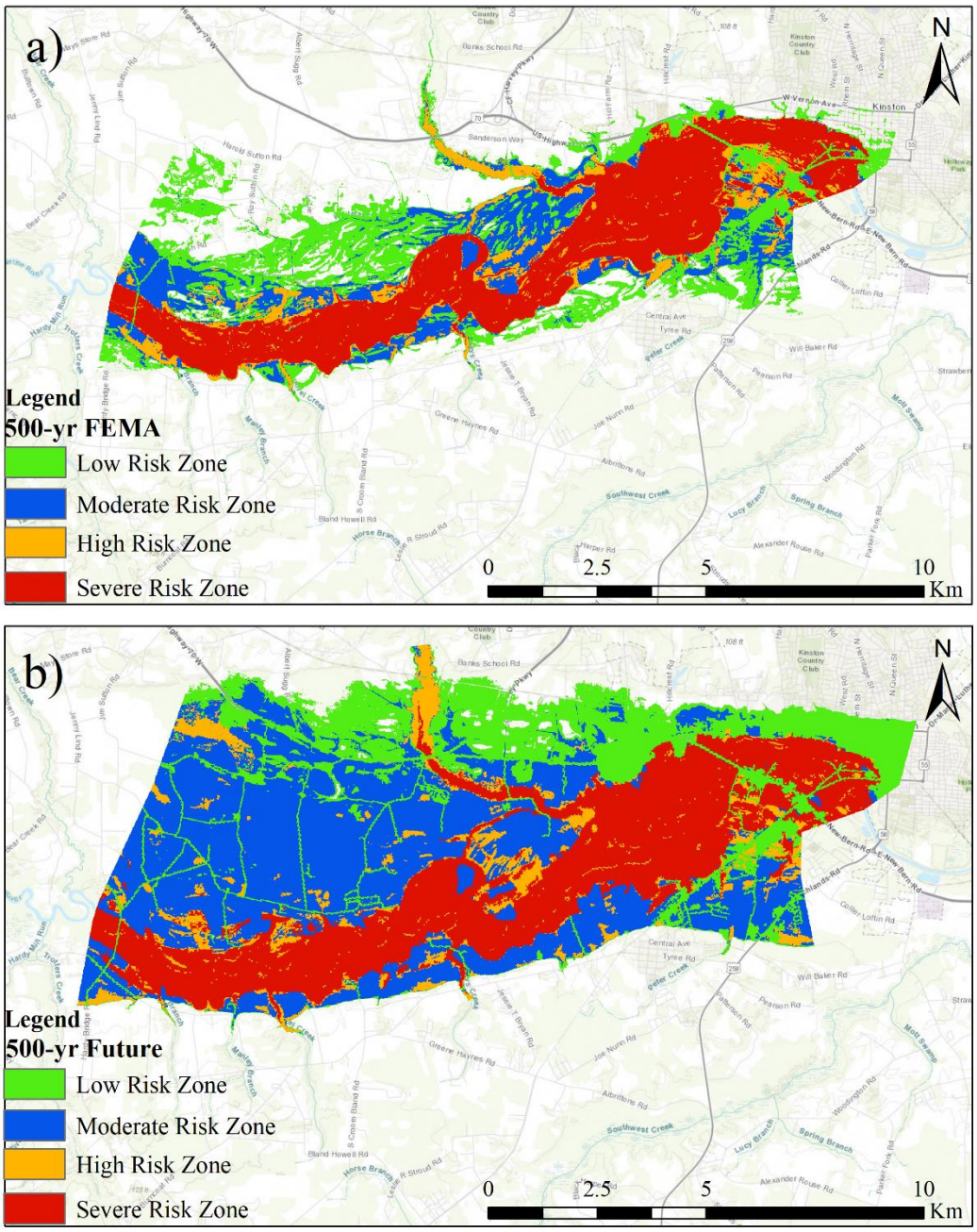

Figure 15: Comparison of extent of risk for 500-year a) existing (FEMA) and b) future scenarios utilizing the risk zonal classifications.

Source: Esri, HERE, Garmin, Intermap, increment P Crop., GEBCO, USGS, FAO, NPS, NRCAN, GeoBase, IGN, Kadaster NL, Ordnance Survey, Esri Japan, METI, Esri China (Hong Kong), swisstopo © OpenStreetMaps contributors, and the GIS User Community.

5.4 Discussion

Flooding can cause colossal damage to human life, settlement, and key infrastructures, resulting in many environmental and socio-economic consequences. The highly urbanized areas located along the floodplain can be at higher risk, even they are highly regulated (Mihu-Pintilie et al., 2019). Moreover, since ancient times, human populations around the globe have predominately lived near water bodies such as seashores or riverbanks to increase the ease of their living. Around 40% of the world population is currently residing within the 100 km periphery of the coastal areas, which is vulnerable to the different water-related disasters such as sea-level rises and storm surges. The consequences related to these disasters would be more severe due to the highly concentrated population and low elevation in the coastal regions. Furthermore, due to the changes in future streamflow, flood-related hazards are likely to increase for coastal cities like Kinston. Likewise, the change in streamflow is inevitable in the future due to the sea level rises and increased global warming. Accordingly, flood protection planning ensuring minimal loss should be introduced in the future to mitigate flood risk effectively. This study utilized the streamflow projections of CMIP6 to analyze the increase in floodplain inundation due to climate change. Furthermore, different emission scenarios provided by CMIP6 were employed to evaluate the future streamflow, including different forcing level and SSP's. Hence, evaluating the future flow helps us analyze the impact of both climatic and societal change (O'Neil et al., 2016), allowing the acknowledgment of a broad range of future streamflow.

For the flood frequency analysis, it is important to use appropriate probability distribution that would be further used to evaluate design floods. For sub-tropical humid climatic conditions, many previous studies suggested the use of GEV as a probability distribution that will likely fit

for the prediction of future streamflow (Re & Barros, 2009; Santos et al., 2016; Shi et al., 2010). Thus, the GEV-Max(L-Moments) was employed for the evaluation of peak flows with different year return period for both existing and future scenarios based on the fact that the climatic condition of a study reach was relevant to that of past research. Within the four different future scenarios, most of them had a DCF value greater than one while considering different return period flood events. These values suggest the future design flow is likely to be higher than the existing flows. The estimated DCF from the multimodel ensemble of four different individual future scenarios is greater than 1, based on the evaluation of the 100-year recurrence interval. The higher DCF generating scenario (SSP5-8.5) was used for this study for the convenience of analysis. For all four scenarios, the design 100-year flow would be nearly double the existing design 100-year flow. The result of the SSP5-8.5 scenario, with the higher DCF among all four scenarios, points to a higher design flow in the future than the existing condition. Moreover, as the DCF increases, the design flow also increases. The SSP5-8.5 scenario is likely to have a higher chance of flooding among all other scenarios, due to higher predicted design flow. Hence, in this study, future scenarios for both the 100-year and 500-year return period flows were analyzed. DCM was used for the estimation of future flows of different scenarios. Then, the design streamflow from selected future scenarios was routed through the HEC-RAS 1D model for the generation of the floodplain inundation maps to compare it with the existing ones.

Since the DCF is higher for the future scenario SSP5-8.5, the increase in the future design flow is also at its maximum level. So, the maximum design flow from the SSP5-8.5 scenario was then employed in the HEC-RAS model for the generation of inundation maps of the study area, Neuse River, NC. The projected future flows were compared with the existing FEMA flows to analyze the impact of climate change in future streamflow. The future 100-year flow was found

to be higher than the existing 500-year flow calculated by FEMA. These results suggest an increase in flood extent in the city of Kinston and a higher possibility of a loss of public infrastructures and damage to human settlement. Previous studies suggested an increase in streamflow of the NRB, as the intensity of precipitation was projected to increases due to climatic scenarios (Arnell & Gosling, 2016; Johnson et al., 2015) For instance, in the last two decades, NC has faced more than three severe hurricanes, resulting in destructive flooding that submerged a portion of the City of Kinston. Previous studies have inferred that the impact of climate change and the change in land use can differ the result of risk analysis, due to change in the extent of the floodplain (Tingsanchali & Karim, 2010 & 2005). This study uses future flows incorporating climate, land use, and socio-economic changes. Most of the population of Kinston is residing on the bank of the Neuse River, which makes the area more vulnerable to flood hazards. The agricultural land near the riverbank is running through the existing floodplain. Future flooding risks not only affecting the settlement of Kinston city but is also predicted to produce a large impact on local agricultural land while causing loss of human life and economic harm. Thus, this study performed a zonal risk analysis based on flood hazard and land use, which has shown the severity of risk in land use. It can help local agencies to make a significant effort on the preparedness of those areas depending on the level of risk. Also, the assessment of flood hazards, vulnerability, and risk would lead to greater mitigation of the risk of future flooding.

The current study managed to evaluate the flood hazard area as well as risk zoning so that the risk map can be prepared to depict all four risk zoning areas. Mapping can be a key factor in mitigating flood risk. Policymakers, engineers, and water resource managers can use the risk maps for the planning and constructing facilities that mitigate the risk of future flooding. The risk analysis showed the vulnerability of the community residing in the bank of the Neuse River and

the fertile land on the bank of the river. Thus, appropriate research is direly needed for the analysis of future flooding in this area. In this study, different historical and future scenarios hydroclimatic data were employed to predict the future streamflow, which incorporates climatic variability in the future. The future design streamflow was used for the assessment of risk, which can be considered during the planning and building the hydraulic structures so that it can minimize the flood risk incorporated with climate change and socio-economic pathways.

CHAPTER 6

SUMMARY AND CONCLUSION

6.1 Summary and Conclusion

This study facilitates the use of different GCMs associated with historical and future scenarios of CMIP6 to estimate the increasing flood risk caused by the changes to streamflow in the future climate. It also shows floodplain changes due to existing and future climatic scenarios. The floodplain area generated using the future climatic scenarios, SSP5-8.5, resulted in nearly two times the floodplain area that is created by existing scenarios for 100-year flood events. This shows the likelihood of an increase in flooding threats under future climate conditions. As manifested by the current change in climate, it is anticipated to increase extreme hydrological events in the future. This will subsequently increase the risk associated with these extremes. The study purposed an approach using different climatic models and observation data that can minimize the adverse impact of change in streamflow in the future. The following points summarize the main conclusion of this study:

a. Bias correction of different scenarios obtained from the multimodel ensemble with the historical data was performed using the CDF-t method. The CDF-t method increases the robustness in evaluating future change in streamflow.
b. For the estimation of the design flow, GEV-Max (L-Moments) was utilized, where SSP5-8.5 was found to have a maximum flow for the 100-year return period.
c. The DCF for most future scenarios were found to be higher than 1, suggesting the increase in future streamflow in comparison with the existing (FEMA) flow.
d. For the 100-year return period flood event, future scenario SSP5-8.5 predicted the maximum increase in the peak flow in Neuse River.

e. HEC-RAS 1D steady modeling was used to simulate the floodplain mapping extent of Neuse River, NC. The result showed a higher extent of flooding for the future 100-year scenario than for the existing FEMA 500-year peak flows.
f. Reclassification and mapping of hazard, vulnerability, and risk were completed utilizing the SSP5-8.5 scenario for the assessment of risk.
g. The extent of different flood risk zone of future flows for 100 and 500-year flood events highlights the increase in potential risk and their severity in the future.

Overall, this research highlights the use of historical and future CMIP6 climate data to forecast the future streamflow for the different return periods. The calculated streamflow is then utilized to develop the future floodplains inundation maps. Using the information from the floodplain maps, a flood risk assessment in terms of a potential threat that can be posed in the study area is performed. As evidenced by the results, the higher GHG emission scenarios are associated with intense future flooding events. These events can pose an adverse effect on the socio-economic factors of the community. On average, flood management structures last for several decades. The structures that are designed using the historic climatic information may not endure future storm events. However, the design of these structures can be optimized by using the forecasted streamflow and by increasing sustainability for future climatic conditions. The forecasting and risk assessment of such catastrophic events helps policymakers to prepare flood risk mitigation plans and a skeleton for making key decisions in the field of water resource management. As an alternative approach, alteration of land use can be suggested to elevate the management of flood risks sustainably.

6.2 Limitations

In this study, a detailed analysis of future flooding is performed that helps to fulfill the objective of the study. However, the limitations are inevitable regarding the current study. The study is performed using CMIP6 climate projections, where the limited number of projections that are made available to date. Since the sixth phase of CMIP6 is continuously working in producing different streamflow data for a different scenario, this study used the data that are updated till date to understand the future flooding in Neuse River, NC. Different scenarios give a varying range of design streamflow. The study utilizes streamflow data to forecast the design peak flow. Moreover, the period of 2036 to 2100 was taken as the study period, whereas further study can also be done using the near future and far future rather than taking the long-range of data so that it can help to provide another aspect on analyzing the flood events.

This study used GCMs that were obtained from CNRM-CERFACS, since it is the only institute to develop the streamflow projection for different future scenarios in CMIP6. However, many studies (Brunner et al., 2020; Camici et al.,2014; Eyring et al., 2016) suggested the use of as many models from different modeling institute as the climate models from the same institution might share similar ideas, code or even sometime full component which might lead to biases in thus produced results. Thus, the study can be done using more GCMs obtained from different modeling center to reduce the biasness and help in generating more robust scenarios to analyze the future change in streamflow.

Also, for the bias correction, the historical 65 year of duration was used where both observed and modeled historical climate data were utilized. Since the CDF-t was utilized to remove the biases in the future climate projection, the shift in extreme events due to climate change might not be included in the bias corrected future climate projection (Pierce et al. 2015).

CHAPTER 7

RECOMMENDATION FOR FUTURE WORKS

The current study is focused on analyzing the streamflow so that it can aid on understand the impact of climate change. Since the CMIP6 data are yet to be made available completely, in the future, different analysis regarding the streamflow projection can be performed using many streamflow data for different scenarios. Moreover, after the completion of phase 6 of CMIP, it is recommended to use the GCMs from different modeling institute in order to minimize the bias that can be generated due to the similarity in the models of same institute. Likewise, in future, decadal and multi-decadal time period can be used for the analysis so that the study can compare the long term impact presented in the study with the short term impact of climate change due to the variability of streamflow. Further, the analysis was performed for the SSP5-8.5 scenario, so for the future study it is suggested to utilize the future scenarios SSP1-2.6, SSP2-4.5, SSP3-7.0 so that it would be very helpful in forecasting the future variation of streamflow.

In this study, the hazard classification was performed based on the United Nation Disaster Relief Organization classifications. Many agencies have their own set of standards to classify hazard, so it is recommended to adopt appropriate classification as per the study area location. Also, this study used land use as a factor for the analysis of flood hazard vulnerability in the study area, however, a lot of factors such as population density, societal factors, urbanization can be taken into account for the detailed study of vulnerability assessment. As this study is more focused on forecasting of flood for a different scenario, it can be suggested to have detail flood assessment using various factors, to make the study more precise. Moreover, for further study the detail assessment of flood hazard, vulnerability, and risk, can be done in separate studies.

REFERENCES

Ahmad, H. F., Alam, A., Bhat, M. S., & Ahmad, S. (2016). One Dimensional Steady Flow Analysis Using HECRAS–A Case of River Jhelum, Jammu and Kashmir. European Scientific Journal, 12(32), 340-350.

Alaghmand, S., bin Abdullah, R., Abustan, I., & Eslamian, S. (2012). Comparison Between Capabilities of HEC-RAS and MIKE11 Hydraulic Models in River Flood Risk Modelling (A Case Study of Sungai Kayu Ara River basin, Malaysia). International Journal of Hydrology Science and Technology, 2(3), 270-291.

Alfieri, L., Bisselink, B., Dottori, F., Naumann, G., de Roo, A., Salamon, P., Wyser, K., & Feyen, L. (2017). Global Projections of River Flood Risk in a Warmer World. Earth's Future, 5(2), 171-182.

Alfieri, L., Feyen, L., Dottori, F., & Bianchi, A. (2015). Ensemble Flood Risk Assessment in Europe Under High End Climate Scenarios. Global Environmental Change, 35, 199-212.

Ali, A. F., Zhang, X. P., Adnan, M., Iqbal, M., & Khan, G. (2018). Projection of Future Streamflow of The Hunza River Basin, Karakoram Range (Pakistan) Using HBV Hydrological Model. Journal of Mountain Science, 15(10), 2218-2235.

Allen, M.R., O.P. Dube, W. Solecki, F. Aragon-Durand, W. Cramer, S. Humphreys, M. Kainuma, J. Kala, N. Mahowald, Y. Mulugetta, R. Perez, M. Wairiu, and K. Zickfeld, 2018:Framing and context. In Global Warming of 1.5 °C. An IPCC Special Report on the Impacts of Global Warming of 1.5 °C above Pre-Industrial Levels and Related Global Greenhouse Gas Emission Pathways, in the Context of Strengthening the Global Response to the Threat of Climate Change, Sustainable Development, and Efforts to Eradicate Poverty; Masson-Delmotte, V.P., Zhai, H.-O., Portner, D., Roberts, J., Skea,

P.R., Shukla, A., Pirani, W., Moufouma-Okia, C., Pean, R., Pidcock, S., et al., Eds.; 2018.In Press.

American Rivers. (December 2019). Retrieved from: https://www.americanrivers:river/neuse-river/

Anjum, M. N., Ding, Y., & Shangguan, D. (2019). Simulation of the projected climate change impacts on the river flow regimes under CMIP5 RCP scenarios in the westerlies dominated belt, northern Pakistan. Atmospheric Research, 227, 233-248.

Arnell, N. W. (1999). Climate change and global water resources. Global Environmental Change, 9, S31-S49.

Arnell, N. W., & Gosling, S. N. (2016). The impacts of climate change on river flood risk at the global scale. Climatic Change, 134(3), 387-401.

Ayuketang Arreyndip, N., & Joseph, E. (2016). Generalized extreme value distribution models for the assessment of seasonal wind energy potential of Debuncha, Cameroon. Journal of Renewable Energy, 2016 (9357812), 9. https://doi.org/10.1155/2016/9357812

Bai, Y., Zhang, Z., & Zhao, W. (2019). Assessing the Impact of Climate Change on Flood Events Using HEC-HMS and CMIP5. Water, Air, & Soil Pollution, 230(6), 119.

Bao, Z., Zhang, J., Yan, X., Wang, G., Jin, J., Liu, Y., & Guan, X. (2019). Future streamflow assessment in the Haihe River basin located in northern China using a regionalized variable infiltration capacity model based on 18 CMIP5 GCMs. Journal of Water and Climate Change. https://doi.org/10.2166/wcc.2019.095

Basheer, A. K., Lu, H., Omer, A., Ali, A. B., & Abdelgader, A. M. (2016). Impacts of climate change under CMIP5 RCP scenarios on the streamflow in the Dinder River and ecosystem habitats in Dinder National Park, Sudan. Hydrology and Earth System

Sciences, 20(4), 1331.

Batchabani, E., Sormain, E., & Fuamba, M. (2016). Potential impacts of projected climate change on flooding in the Riviere des Prairies basin, Quebec, Canada: One-dimensional and two-dimensional simulation-based approach. Journal of Hydrologic Engineering, 21(12), 05016032-1-19.

Bathi, J. R., & Das, H. S. (2016). Vulnerability of coastal communities from storm surge and flood disasters. International Journal of Environmental Research and Public Health, 13(2), 239.

Bhandari, R., Kalra, A., & Kumar, S. (2020). Analyzing the effect of CMIP5 climate projections on streamflow within the Pajaro River Basin. Open Water Journal, 6(1), 5 (1-25).

Bjurström, A., & Polk, M. (2011). Physical and economic bias in climate change research: a scientometric study of IPCC Third Assessment Report. Climatic Change, 108(1-2), 1-22.

Block, P. J., Souza Filho, F. A., Sun, L., & Kwon, H. H. (2009). A streamflow forecasting framework using multiple climate and hydrological models 1. Journal of the American Water Resources Association, 45(4), 828-843.

Bosshard, T., Kotlarski, S., Zappa, M., & Schär, C. (2014). Hydrological climate-impact projections for the Rhine River: GCM–RCM uncertainty and separate temperature and precipitation effects. Journal of Hydrometeorology, 15(2), 697-713.

Brunner, G.W. (2016). HEC-RAS, River Analysis System Hydraulic Reference Manual, Version 5.0; US Army Corps of Engineers:Davis, CA, USA, 2016; pp. 3–538.

Camici, S., Brocca, L., Melone, F., & Moramarco, T. (2014). Impact of climate change on flood frequency using different climate models and downscaling approaches. Journal of

Hydrologic Engineering, 19(8), 04014002 (1-15).

Cannon, A. J., Sobie, S. R., & Murdock, T. Q. (2015). Bias correction of GCM precipitation by quantile mapping: How well do methods preserve changes in quantiles and extremes?. Journal of Climate, 28(17), 6938-6959.

Chattopadhyay, S., & Jha, M. K. (2016). Hydrological response due to projected climate variability in Haw River watershed, North Carolina, USA. Hydrological Sciences Journal, 61(3), 495-506.

Chen, C., Kalra, A., & Ahmad, S. (2019). Hydrologic responses to climate change using downscaled GCM data on a watershed scale. Journal of Water and Climate Change, 10(1), 63-77.

Chen, Y., Liu, A., & Cheng, X. (2020). Quantifying economic impacts of climate change under nine future emission scenarios within CMIP6. Science of The Total Environment, 703, 134950.

Christensen, J. H., Boberg, F., Christensen, O. B., & Lucas-Picher, P. (2008). On the need for bias correction of regional climate change projections of temperature and precipitation. Geophysical Research Letters, 35(20), 1-6.

Cook, A., & Merwade, V. (2009). Effect of topographic data, geometric configuration and modeling approach on flood inundation mapping. Journal of hydrology, 377(1-2), 131-142.

Cook, B. I., Mankin, J. S., Marvel, K., Williams, A. P., Smerdon, J. E., & Anchukaitis, K. J. (2020). Twenty-First Century Drought Projections in the CMIP6 Forcing Scenarios. Earth's Future, 8(6), 1-21.

De Paola, F., Giugni, M., Pugliese, F., Annis, A., & Nardi, F. (2018). GEV parameter estimation

and stationary vs. non-stationary analysis of extreme rainfall in African test cities. Hydrology, 5(2), 28 (1-23).

Diallo, I., Sylla, M. B., Giorgi, F., Gaye, A. T., & Camara, M. (2012). Multimodel GCM-RCM ensemble-based projections of temperature and precipitation over West Africa for the early 21st century. International Journal of Geophysics, 2012.

DOE, Lawrence Livermore National Laboratory. (2019). Retrieved from: https://esgf-node.llnl.gov/search/cmip6/

Duran-Encalada, J. A., Paucar-Caceres, A., Bandala, E. R., & Wright, G. H. (2017). The impact of global climate change on water quantity and quality: A system dynamics approach to the US–Mexican transborder region. European Journal of Operational Research, 256(2), 567-581.

Easterling, D. R., Meehl, G. A., Parmesan, C., Changnon, S. A., Karl, T. R., & Mearns, L. O. (2000). Climate extremes: observations, modeling, and impacts. science, 289(5487), 2068-2074.

Encyclopedia Britannica. (December 2019) Retrieved from: https://www.britannica.com/place/Neuse-River

Eyring, V., Bony, S., Meehl, G. A., Senior, C. A., Stevens, B., Stouffer, R. J., & Taylor, K. E. (2016). Overview of the Coupled Model Intercomparison Project Phase 6 (CMIP6) experimental design and organization. Geoscientific Model Development, 9(5), 1937-1958.

Famien, A. M., Janicot, S., Ochou, A. D., Vrac, M., Defrance, D., Sultan, B., & Noel, T. (2018). A bias-corrected CMIP5 dataset for Africa using the CDF-t method: a contribution to agricultural impact studies.

FEMA. (2009). NFIP Guidebook. Retrieved from: https://www.fema.gov/media-library-data/20130726-1647-20490-1041/nfipguidebook_5edition_web.pdf

FEMA. (2018, November). Guidance for Flood Risk Analysis and Mapping, Accepting Numerical Models for Use in the NFIP. Retrieved from: https://www.fema.gov/media-library-data/1537888714503-3f556061b84f26b86d286513240e8dd4/Guidance_Accepting_Numerical_Models_for_Use_in_the_NFIP_(Feb_2018).pdf

FEMA. (2019, November). Guidance for Flood Risk Analysis and Mapping. Retrieved from: https://www.fema.gov/media-library-data/1578062957793-0274cb6a7a3801a07a3db7916e64e80d/FloodwayAnalysis_and_Mapping_Nov_2019.pdf

FIS. (April, 2013). A Report of Hazard in Lenoir County, North Carolina and Incorporated Areas. Retrieved from: https://fris.nc.gov/FRIS_WS/PDF/5e19eaf2b15b4aefa17344e46a19c500.pdf

Ford, T. W., Quiring, S. M., Thakur, B., Jogineedi, R., Houston, A., Yuan, S., A., Kalra & Lock, N. (2018). Evaluating soil moisture–precipitation interactions using remote sensing: a sensitivity analysis. Journal of Hydrometeorology, 19(8), 1237-1253.

Gao, J., Sheshukov, A. Y., Yen, H., Douglas-Mankin, K. R., White, M. J., & Arnold, J. G. (2019). Uncertainty of hydrologic processes caused by bias-corrected CMIP5 climate change projections with alternative historical data sources. Journal of Hydrology, 568, 551-561.

Gao, P., Carbone, G. J., & Guo, D. (2016). Assessment of NARCCAP model in simulating rainfall extremes using a spatially constrained regionalization method. International Journal of Climatology, 36(5), 2368-2378.

Gosling, S. N., & Arnell, N. W. (2016). A global assessment of the impact of climate change on water scarcity. Climatic Change, 134(3), 371-385.

Griffin, M. T., Montz, B. E., & Arrigo, J. S. (2013). Evaluating climate change induced water stress: A case study of the Lower Cape Fear basin, NC. Applied Geography, 40, 115-128.

Guo, L. Y., Gao, Q., Jiang, Z. H., & Li, L. (2018). Bias correction and projection of surface air temperature in LMDZ multiple simulation over central and eastern China. Advances in Climate Change Research, 9(1), 81-92.

Guo, L., Jiang, Z., Chen, D., Le Treut, H., & Li, L. (2020). Projected precipitation changes over China for global warming levels at 1.5° C and 2° C in an ensemble of regional climate simulations: impact of bias correction methods. Climatic Change, 1-21.

Gupta, V., Singh, V., & Jain, M. K. (2020). Assessment of precipitation extremes in India during the 21st century under SSP1-1.9 mitigation scenarios of CMIP6 GCMs. Journal of Hydrology, 125422.

Hall, K. Expected Costs of Damage from Hurricane Winds and Storm-Related Flooding; Congressional Budget Office Document number 55019: Washington, DC, USA, 2019; 48 Pages.

Hamzah, F. M., Yusoff, S. H. M., & Jaafar, O. (2019). L-Moment-Based Frequency Analysis of High-Flow at Sungai Langat, Kajang, Selangor, Malaysia. Sains Malaysiana, 48(7), 1357-1366.

Hay, L. E., Wilby, R. L., & Leavesley, G. H. (2000). A comparison of delta change and downscaled GCM scenarios for three mountainous basins in the United States 1. JAWRA Journal of the American Water Resources Association, 36(2), 387-397.

Hirabayashi, Y., Kanae, S., Emori, S., Oki, T., & Kimoto, M. (2008). Global projections of

changing risks of floods and droughts in a changing climate. Hydrological Sciences Journal, 53(4), 754-772.

Hirpa, F. A., Alfieri, L., Lees, T., Peng, J., Dyer, E., & Dadson, S. J. (2019). Streamflow response to climate change in the Greater Horn of Africa. Climatic Change, 156(3), 341-363.

Hoan, N. X., Khoi, D. N., & Nhi, P. T. T. (2020). Uncertainty assessment of streamflow projection under the impact of climate change in the Lower Mekong Basin: a case study of the Srepok River Basin, Vietnam. Water and Environment Journal, 34(1), 131-142.

Hosking, J.R.M. (1990). L-moments: Analysis and Estimation of Distributions Using Linear Combinations of Order Statistics. Journal of the Royal Statistical Society, 52(1), 105-124.

Hosking, J. R. M., & Wallis, J. R. (2005). Regional frequency analysis: an approach based on L-moments. Cambridge university press.

Hosking, J. R. M., Wallis, J. R., & Wood, E. F. (1985). Estimation of the generalized extreme-value distribution by the method of probability-weighted moments. Technometrics, 27(3), 251-261.

Huang, J., Zhang, J., Zhang, Z., Xu, C., Wang, B., & Yao, J. (2011). Estimation of future precipitation change in the Yangtze River basin by using statistical downscaling method. Stochastic Environmental Research and Risk Assessment, 25(6), 781-792.

Johnson, T., Butcher, J., Deb, D., Faizullabhoy, M., Hummel, P., Kittle, J., McGinnis, S., Mearns, L.O., Nover, D., Parker, A., Sarkar, S., Srinivasan, R., Tuppad, P., Warren, M., Weaver, C., & Witt, J. (2015). Modeling streamflow and water quality sensitivity to climate change and urban development in 20 US watersheds. Journal of the American Water Resources Association, 51(5), 1321-1341.

Joshi, N., Bista, A., Pokhrel, I., Kalra, A., & Ahmad, S. (2019a). Rainfall-Runoff Simulation in Cache River Basin, Illinois, Using HEC-HMS. In World Environmental and Water Resources Congress 2019: Watershed Management, Irrigation and Drainage, and Water Resources Planning and Management (pp. 348-360). Reston, VA: American Society of Civil Engineers.

Joshi, N., Rahaman, M. M., Thakur, B., Shrestha, A., Kalra, A., & Gupta, R. (2020a). Assessing the Effects of Climate Variability on Groundwater in Northern India. In World Environmental and Water Resources Congress 2020: Groundwater, Sustainability, Hydro-Climate/Climate Change, and Environmental Engineering (pp. 41-52). Reston, VA: American Society of Civil Engineers.

Joshi, N., Tamaddun, K., Parajuli, R., Kalra, A., Maheshwari, P., Mastino, L., & Velotta, M. (2020b). Future Changes in Water Supply and Demand for Las Vegas Valley: A System Dynamic Approach based on CMIP3 and CMIP5 Climate Projections. Hydrology, 7(1), 16.

Joshi, N., Kalra, A., & Lamb, K. W (2020c). Land–Ocean–Atmosphere Influences on Groundwater Variability in the South Atlantic–Gulf Region, Hydrology, 7(4), 71.

Joshi, N., Kalra, A., Thakur, B., Lamb, K., & Bhandari, S.(2020d). Persistence and shift detection in sea level records along the US coast: Is sea level rising? Hydrology. (In Review).

Joshi, N., Lamichhane, G. R., Rahaman, M. M., Kalra, A., & Ahmad, S. (2019b). Application of HEC-RAS to Study the Sediment Transport Characteristics of Maumee River in Ohio. In World Environmental and Water Resources Congress 2019: Hydraulics, Waterways, and Water Distribution Systems Analysis (pp. 257-267). Reston, VA: American Society of

Civil Engineers.

Joshi, N., & Dongol, R. (2018). Severity of Climate Induced Drought and its Impact on Migration: A Study of Ramechhap District, Nepal.

Kalra, A., & Ahmad, S. (2009). Using oceanic-atmospheric oscillations for long lead time streamflow forecasting. Water Resources Research, 45(3), 1-18.

Kalra, A., Joshi, N., Baral, S., Pradhan, S., Paudel S., Xia, C, Mambepa, M., Gupta, R. (2020a) Coupled 1D and 2D HEC-RAS Floodplain Modelling of Pecos River in New Mexico. In World Environmental and Water Resources Congress 2021. (Abstract).

Kalra, A., Li, L., Li, X., & Ahmad, S. (2013). Improving streamflow forecast lead time using oceanic-atmospheric oscillations for Kaidu river basin, Xinjiang, china. Journal of Hydrologic Engineering, 18(8), 1031-1040.

Kalra, A., Piechota, T. C., Davies, R., & Tootle, G. A. (2008). Changes in US streamflow and western US snowpack. Journal of Hydrologic Engineering, 13(3), 156-163.

Kalra, A., Joshi, N., Pokhrel, I., Pradhan, S., Adhikari P., Xia, C, Gupta, R. (2020b) Assessment of Floodplain inundation mapping of Davenport City in Iowa using CIVIL Geo-HECRAS. In World Environmental and Water Resources Congress 2021. (Abstract).

Kalra, A., Sagarika, S., Pathak, P., & Ahmad, S. (2017). Hydro-climatological changes in the Colorado River Basin over a century. Hydrological Sciences Journal, 62(14), 2280-2296.

Karamouz, M., Zahmatkesh, Z., Goharian, E., & Nazif, S. (2015). Combined impact of inland and coastal floods: Mapping knowledge base for development of planning strategies. Journal of Water Resources Planning and Management, 141(8), 04014098.

Kasiviswanathan, K. S., He, J., & Tay, J. H. (2017). Flood frequency analysis using multi-objective optimization based interval estimation approach. Journal of Hydrology, 545,

251-262.

Kay, A. L., Davies, H. N., Bell, V. A., & Jones, R. G. (2009). Comparison of uncertainty sources for climate change impacts: flood frequency in England. Climatic change, 92(1-2), 41-63.

Kelly, C. N., McGuire, K. J., Miniat, C. F., & Vose, J. M. (2016). Streamflow response to increasing precipitation extremes altered by forest management. Geophysical Research Letters, 43(8), 3727-3736.

Kendon, E. J., Jones, R. G., Kjellström, E., & Murphy, J. M. (2010). Using and designing GCM–RCM ensemble regional climate projections. Journal of Climate, 23(24), 6485-6503.

Khalyani, A. H., Gould, W. A., Harmsen, E., Terando, A., Quinones, M., & Collazo, J. A. (2016). Climate change implications for tropical islands: Interpolating and interpreting statistically downscaled GCM projections for management and planning. Journal of Applied Meteorology and Climatology, 55(2), 265-282.

Klijn, F., Kreibich, H., De Moel, H., & Penning-Rowsell, E. (2015). Adaptive flood risk management planning based on a comprehensive flood risk conceptualisation. *Mitigation and Adaptation Strategies for Global Change*, *20*(6), 845-864.

Koirala, S., Hirabayashi, Y., Mahendran, R., & Kanae, S. (2014). Global assessment of agreement among streamflow projections using CMIP5 model outputs. Environmental Research Letters, 9(6), 064017.

Kumar, N., Lal, D., Sherring, A., & Issac, R. K. (2017). Applicability of HEC-RAS & GFMS tool for 1D water surface elevation/flood modeling of the river: a Case Study of River Yamuna at Allahabad (Sangam), India. Modeling Earth Systems and Environment, 3(4), 1463-1475.

Kuntiyawichai, K., Sri-Amporn, W., Wongsasri, S., & Chindaprasirt, P. (2020). Anticipating of

Potential Climate and Land Use Change Impacts on Floods: A Case Study of the Lower Nam Phong River Basin. Water, 12(4), 1158.

Li, H., Sheffield, J., & Wood, E. F. (2010). Bias correction of monthly precipitation and temperature fields from Intergovernmental Panel on Climate Change AR4 models using equidistant quantile matching. Journal of Geophysical Research: Atmospheres, 115(D10).

Li, L. J., Zhang, L., Wang, H., Wang, J., Yang, J. W., Jiang, D. J., ... & Qin, D. Y. (2007). Assessing the impact of climate variability and human activities on streamflow from the Wuding River basin in China. Hydrological Processes: An International Journal, 21(25), 3485-3491.

Lim, N. J. (2011). Performance and uncertainty estimation of 1-and 2-dimensional flood models.

López-Ballesteros, A., Senent-Aparicio, J., Martínez, C., & Pérez-Sánchez, J. (2020). Assessment of future hydrologic alteration due to climate change in the Aracthos River basin (NW Greece). Science of The Total Environment, 733,139299.

Maheshwari, P., Khaddar, R., Kachroo, P., & Paz, A. (2016). Dynamic modeling of performance indices for planning of sustainable transportation systems. Networks and Spatial Economics, 16(1), 371-393.

Maheshwari, P., Kachroo, P., Paz, A., & Khaddar, R. (2015). Development of control models for the planning of sustainable transportation systems. Transportation Research Part C: Emerging Technologies, 55, 474-485.

Meehl, G. A., Moss, R., Taylor, K. E., Eyring, V., Stouffer, R. J., Bony, S., & Stevens, B. (2014). Climate model intercomparisons: Preparing for the next phase. Eos, Transactions American Geophysical Union, 95(9), 77-78.

Mehta, D. J., Ramani, M. M., & Joshi, M. M. (2013). Application of 1-D HEC-RAS model in

design of channels. Methodology, 1(7), 4-62.

Merz, B., Aerts, J. C. J. H., Arnbjerg-Nielsen, K., Baldi, M., Becker, A., Bichet, A., ... & Delgado, J. M., G. Blöschl, G., Bouwer, L.M., Brauer, A., Cioffi, F., Delgado, J.M., Gocht, M., Guzzetti, F., Harrigan, S., Hirschboeck, K., Kilsby, C., Kron, W., Kwon, H-H., Lall, U., Merz, R., Nissen, K., Salvatti1, P., Swierczynski, T., Ulbrich, U., Viglione, A., Ward, P.J., Weiler, M., Wilhelm, B., & Nied, M. (2014).,Floods and climate: emerging perspectives for flood risk assessment and management. Natural Hazards and Earth System Sciences, 14(7), 1921-1942.

Michelangeli, P.A.; Vrac, M.; Loukos, H. Probabilistic downscaling approaches: Application to wind cumulative distribution functions. Geophysical Research Letter, 36(11). doi:10.1029/2009GL038401.

Middelkoop, H., Daamen, K., Gellens, D., Grabs, W., Kwadijk, J. C., Lang, H., ... & Wilke, K. (2001). Impact of climate change on hydrological regimes and water resources management in the Rhine basin. Climatic Change, 49(1-2), 105-128.

Mihu-Pintilie, A., Cîmpianu, C. I., Stoleriu, C. C., Pérez, M. N., & Paveluc, L. E. (2019). Using High-Density LiDAR Data and 2D Streamflow Hydraulic Modeling to Improve Urban Flood Hazard Maps: A HEC-RAS Multi-Scenario Approach. Water, 11(9), 1832.

Mishra, V., Bhatia, U., & Tiwari, A. D. (2020). Bias-corrected climate projections from Coupled Model Intercomparison Project-6 (CMIP6) for South Asia. arXiv preprint arXiv:2006.12976.

Moradkhani, H., Baird, R. G., & Wherry, S. A. (2010). Assessment of climate change impact on floodplain and hydrologic ecotones. Journal of hydrology, 395(3-4), 264-278.

Mukundan, R., Acharya, N., Gelda, R. K., Frei, A., & Owens, E. M. (2019). Modeling

streamflow sensitivity to climate change in New York City water supply streams using a stochastic weather generator. Journal of Hydrology: Regional Studies, 21, 147-158.

MRLC (2016). Retrieved from: https://www.mrlc.gov/data?f%5B0%5D=category%3Aland%20cover

Neff, R., Chang, H., Knight, C. G., Najjar, R. G., Yarnal, B., & Walker, H. A. (2000). Impact of climate variation and change on Mid-Atlantic Region hydrology and water resources. Climate Research, 14(3), 207-218.

Ngigi, S. N. (2009). Climate change adaptation strategies: water resources management options for smallholder farming systems in sub-Saharan Africa. New York, NY: The Earth Institute at Columbia University.

Nohara, D., Kitoh, A., Hosaka, M., & Oki, T. (2006). Impact of climate change on river discharge projected by multimodel ensemble. Journal of Hydrometeorology, 7(5), 1076-1089.

Norén, V., Hedelin, B., Nyberg, L., & Bishop, K. (2016). Flood risk assessment–practices in flood prone Swedish municipalities. International Journal of Disaster Risk Reduction, 18, 206-217.

Nyaupane, N., Mote, S. R., Bhandari, M., Kalra, A., & Ahmad, S. (2018a). Rainfall-Runoff Simulation Using Climate Change Based Precipitation Prediction in HEC-HMS Model for Irwin Creek, Charlotte, North Carolina. In World Environmental and Water Resources Congress 2018: Watershed Management, Irrigation and Drainage, and Water Resources Planning and Management (pp. 352-363). Reston, VA: American Society of Civil Engineers.

Nyaupane, N., Thakur, B., Kalra, A., & Ahmad, S. (2018b). Evaluating future flood scenarios

using CMIP5 climate projections. Water, 10(12), 1866.

Nyaupane, N., Bhandari, S., Rahaman, M. M., Wagner, K., Kalra, A., Ahmad, S., & Gupta, R. (2018c). Flood frequency analysis using generalized extreme value distribution and floodplain mapping for hurricane Harvey in Buffalo Bayou. In World Environmental and Water Resources Congress 2018: Watershed Management, Irrigation and Drainage, and Water Resources Planning and Management (pp. 364-375). Reston, VA: American Society of Civil Engineers.

NWS (2020). Tropical Cyclones Climatology 1851 – 2016. Retrieved from: https://www.weather.gov/mhx//TropicalClimatology

O'Connor, J. E., & Costa, J. E. (2003). Large floods in the United States: Where they happen and why. Geological Survey (USGS).

Oguntunde, P. G., & Abiodun, B. J. (2013). The impact of climate change on the Niger River Basin hydroclimatology, West Africa. Climate Dynamics, 40(1-2), 81-94.

Okkan, U., & Kirdemir, U. (2016). Downscaling of monthly precipitation using CMIP5 climate models operated under RCPs. Meteorological Applications, 23(3), 514-528.

O'Neill, B. C., Tebaldi, C., Van Vuuren, D. P., Eyring, V., Friedlingstein, P., Hurtt, G., Knutti, R., Kriegler, E., Lamarque, JF., Lowe, J., Moss, R., Riahi, K., Sanderson, BM., & Meehl, G.A. (2016). The scenario model intercomparison project (ScenarioMIP) for CMIP6. European Geosciences Union, 9, 3461 – 3482

Paz, A., Maheshwari, P., Kachroo, P., & Ahmad, S. (2013). Estimation of performance indices for the planning of sustainable transportation systems. Advances in Fuzzy Systems, 2013.

Peng, A., & Liu, F. (2019). Flooding simulation due to Hurricane Florence in North Carolina with HEC RAS. Atmospheric and Oceanic Physics , 1-14. Available on :

https://arxiv.org/pdf/1911.09525v1.pdf

Perez, J., Menendez, M., Mendez, F. J., & Losada, I. J. (2014). Evaluating the performance of CMIP3 and CMIP5 global climate models over the north-east Atlantic region. Climate Dynamics, 43(9-10), 2663-2680.

Pierce, D. W., Cayan, D. R., Maurer, E. P., Abatzoglou, J. T., & Hegewisch, K. C. (2015). Improved bias correction techniques for hydrological simulations of climate change. Journal of Hydrometeorology, 16(6), 2421-2442.

Pinos, J., Timbe, L., & Timbe, E. (2019). Evaluation of 1D hydraulic models for the simulation of mountain fluvial floods: a case study of the Santa Bárbara River in Ecuador. Water Practice and Technology, 14(2), 341-354.

Pokhrel, I., Kalra, A., Rahaman, M. M., & Thakali, R. (2020). Forecasting of Future Flooding and Risk Assessment under CMIP6 Climate Projection in Neuse River, North Carolina. Forecasting, 2(3), 323-346.

Prudhomme, C., Reynard, N., & Crooks, S. (2002). Downscaling of global climate models for flood frequency analysis: where are we now?. Hydrological processes, 16(6), 1137-1150.

Qi, S., Sun, G., Wang, Y., McNulty, S. G., & Myers, J. M. (2009). Streamflow response to climate and landuse changes in a coastal watershed in North Carolina. American Society of Agricultural and Biological Engineers, 52(3), 739-749.

Rahaman, M. M., Lamichhane, G. R., Shrestha, A., Thakur, B., Kalra, A., & Ahmad, S. (2019). Using SWAT to Simulate Streamflow in Trinity River Basin, Texas, USA. In World Environmental and Water Resources Congress 2019: Watershed Management, Irrigation and Drainage, and Water Resources Planning and Management (pp. 421-435). Reston, VA: American Society of Civil Engineers.

Re, M., & Barros, V. R. (2009). Extreme rainfalls in se South America. Climatic Change, 96(1-2), 119-136.

Reshmidevi, T. V., Kumar, D. N., Mehrotra, R., & Sharma, A. (2018). Estimation of the climate change impact on a catchment water balance using an ensemble of GCMs. Journal of Hydrology, 556, 1192-1204.

Riahi, K., Van Vuuren, D. P., Kriegler, E., Edmonds, J., O'neill, B. C., Fujimori, S., ... & Lutz, W. (2017). The shared socioeconomic pathways and their energy, land use, and greenhouse gas emissions implications: an overview. Global Environmental Change, 42, 153-168.

Roy, L., Leconte, R., Brissette, F. P., & Marche, C. (2001). The impact of climate change on seasonal floods of a southern Quebec River Basin. Hydrological Processes, 15(16), 3167-3179.

Ruiter, A. (2012). Delta-change approach for CMIP5 GCMs. Trainee report, Royal Netherlands Meteorological Institute.

Saksena, S., & Merwade, V. (2015). Incorporating the effect of DEM resolution and accuracy for improved flood inundation mapping. Journal of Hydrology, 530, 180-194.

Salvi, K.; Kannan, S.; Ghosh, S. (2011). Statistical downscaling and bias-correction for projections of Indian rainfall and temperature in climate change studies. In Proceedings of the 4th International Conference on Environmental and Computer Science, Singapore, 11, 16–18.

Santos, E. B., Lucio, P. S., & e Silva, C. M. S. (2016). Estimating return periods for daily precipitation extreme events over the Brazilian Amazon. Theoretical and applied climatology, 126(3-4), 585-595.

Selvanathan, S., Sreetharan, M., Lawler, S., Rand, K., Choi, J., & Mampara, M. (2018). A framework to develop nationwide flooding extents using climate models and assess forecast potential for flood resilience. Journal of the American Water Resources Association, 54(1), 90-103

Setegn, S. G., Rayner, D., Melesse, A. M., Dargahi, B., & Srinivasan, R. (2011). Impact of climate change on the hydroclimatology of Lake Tana Basin, Ethiopia. American Geophysical Union, 47(4), 1-13.

ShahiriParsa, A., Noori, M., Heydari, M., & Rashidi, M. (2016). Floodplain zoning simulation by using HEC-RAS and CCHE2D models in the Sungai Maka river. Air, Soil and Water Research, 9, ASWR-S36089, 55-62.

Shi, P., Chen, X., Qu, S. M., Zhang, Z. C., & Ma, J. L. (2010). Regional frequency analysis of low flow based on L moments: Case study in Karst area, Southwest China. Journal of Hydrologic Engineering, 15(5), 370-377.

Shrestha, A., Bhattacharjee, L., Baral, S., Thakur, B., Joshi, N., Kalra, A., & Gupta, R. (2020a). Understanding Suitability of MIKE 21 and HEC-RAS for 2D Floodplain Modeling. In World Environmental and Water Resources Congress 2020: Hydraulics, Waterways, and Water Distribution Systems Analysis (pp. 237-253). Reston, VA: American Society of Civil Engineers.

Shrestha, A., Rahaman, M. M., Kalra, A., Jogineedi, R., & Maheshwari, P. (2020b). Climatological Drought Forecasting Using Bias Corrected CMIP6 Climate Data: A Case Study for India. Forecasting, 2(2), 59-84.

Shrestha, A., Rahaman, M. M., Kalra, A., Thakur, B., Lamb, K. W., & Maheshwari, P. (2020). Regional Climatological Drought: An Assessment Using High-Resolution Data.

Hydrology, 7(2), 33.

Sillmann, J., Kharin, V. V., Zwiers, F. W., Zhang, X., & Bronaugh, D. (2013). Climate extremes indices in the CMIP5 multimodel ensemble: Part 2. Future climate projections. Journal of Geophysical Research: Atmospheres, 118(6), 2473-2493.

Solomon, S., Manning, M., Marquis, M., & Qin, D. (2007). Climate change 2007-the physical science basis: Working group I contribution to the fourth assessment report of the IPCC (Vol. 4). Cambridge university press.

Stefanidis, S., & Stathis, D. (2013). Assessment of flood hazard based on natural and anthropogenic factors using analytic hierarchy process (AHP). Natural Hazards, 68(2), 569-585.

Stewart, S.R.; Berg, R. National Hurricane Center Tropical Cyclone Report Hurricane Florence (AL062018); National Hurricane Centre: Miami, FL, USA, 2019; pp. 2–98.

Stouffer, R. J., Eyring, V., Meehl, G. A., Bony, S., Senior, C., Stevens, B., & Taylor, K. E. (2017). CMIP5 scientific gaps and recommendations for CMIP6. Bulletin of the American Meteorological Society, 98(1), 95-105.

Tamaddun, K. A., Kalra, A., & Ahmad, S. (2017). Wavelet analyses of western US streamflow with ENSO and PDO. Journal of Water and Climate Change, 8(1), 26-39.

Teegavarapu, R. S., Salas, J. D., & Stedinger, J. R. (Eds.). (2019). Statistical Analysis of Hydrologic Variables: Methods and Applications. ASCE.

Thakali, R., Kalra, A., & Ahmad, S. (2016). Understanding the effects of climate change on urban stormwater infrastructures in the Las Vegas Valley. Hydrology, 3(4), 1-16.

Thakali, R., Kalra, A., Ahmad, S., & Qaiser, K. (2018). Management of an urban stormwater system using projected future scenarios of climate models: a watershed-based modeling

approach. Open Water Journal, 5(2), 1-16.

Thakur, B., Kalra, A., Lakshmi, V., Lamb, K. W., Miller, W. P., & Tootle, G. (2020a). Linkage between ENSO phases and western US snow water equivalent. Atmospheric Research, 236, 1-10.

Thakur, B., Kalra, A., Ahmad, S., Lamb, K. W., & Lakshmi, V. (2020b). Bringing statistical learning machines together for hydro-climatological predictions-Case study for Sacramento San joaquin River Basin, California. Journal of Hydrology: Regional Studies, 27, 100651.

Thomas, N., & Nigam, S. (2018). Twentieth-century climate change over Africa: Seasonal hydroclimate trends and sahara desert expansion. Journal of Climate, 31(9), 3349-3370.

Tingsanchali, T., & Karim, F. (2010). Flood-hazard assessment and risk-based zoning of a tropical flood plain: case study of the Yom River, Thailand. Hydrological Sciences Journal–Journal des Sciences Hydrologiques, 55(2), 145-161.

Tingsanchali, T., & Karim, M. F. (2005). Flood hazard and risk analysis in the southwest region of Bangladesh. Hydrological Processes: An International Journal, 19(10), 2055-2069.

US Climate Data. (December 2019). Retrieved from: https://www.usclimatedata.com/climate/kinston/north-carolina/united-states/usnc0359

Vrac, M., Noël, T., & Vautard, R. (2016). Bias correction of precipitation through Singularity Stochastic Removal: Because occurrences matter. Journal of Geophysical Research: Atmospheres, 121(10), 5237-5258.

Wang, L., & Chen, W. (2014). Equiratio cumulative distribution function matching as an improvement to the equidistant approach in bias correction of precipitation. Atmospheric Science Letters, 15(1), 1-6.

Wilby, R. L., & Harris, I. (2006). A framework for assessing uncertainties in climate change impacts: Low-flow scenarios for the River Thames, UK. Water Resources Research, 42(2), 1-10.

Wilby, R. L., Charles, S. P., Zorita, E., Timbal, B., Whetton, P., & Mearns, L. O. (2004). Guidelines for use of climate scenarios developed from statistical downscaling methods. Supporting material of the Intergovernmental Panel on Climate Change, available from the DDC of IPCC TGCIA,1(2), 1-27.

Wilby, R. L., Wigley, T. M. L., Conway, D., Jones, P. D., Hewitson, B. C., Main, J., & Wilks, D. S. (1998). Statistical downscaling of general circulation model output: A comparison of methods. Water Resources Research, 34(11), 2995-3008.

World Bank. (2017). Retrieved from https://www.worldbank.org/en/topic/waterresourcesmanagement. Accessed on: August 10,2020.

Yang, J., Townsend, R. D., & Daneshfar, B. (2006). Applying the HEC-RAS model and GIS techniques in river network floodplain delineation. Canadian Journal of Civil Engineering, 33(1), 19-28.

Yang, X., Wood, E. F., Sheffield, J., Ren, L., Zhang, M., & Wang, Y. (2018). Bias correction of historical and future simulations of precipitation and temperature for China from CMIP5 models. Journal of Hydrometeorology, 19(3), 609-623.

Yonehara, S., & Kawasaki, A. (2020). Assessment of the tidal effect on flood inundation in a low-lying river basin under composite future scenarios. Journal of Flood Risk Management, 13(3), 1-12.

Yuan, F., Tung, Y. K., & Ren, L. (2016). Projection of future streamflow changes of the Pearl

River basin in China using two delta-change methods. Hydrology Research, 47(1), 217-238.

Yuan, X., & Wood, E. F. (2012). Downscaling precipitation or bias-correcting streamflow? Some implications for coupled general circulation model (CGCM)-based ensemble seasonal hydrologic forecast. Water Resources Research, 48(12), 1-7.

Zhai, J., Mondal, S. K., Fischer, T., Wang, Y., Su, B., Huang, J., ... & Uddin, M. J. (2020). Future drought characteristics through a multi-model ensemble from CMIP6 over South Asia. Atmospheric Research, 246, 1-18.

VITA

Graduate School
Southern Illinois University

Indira Pokhrel

indirapokhrel12@gmail.com

Tribhuvan University, Kathmandu, Nepal
Bachelor's in Engineering, Civil Engineering, January 2017

Thesis Paper Title:
ANALYZING THE STREAMFLOW FOR FUTURE FLOODING AND RISK ASSESSMENT UNDER CMIP6 CLIMATE PROJECTION

Major Professor: Dr. Ajay Kalra

Publications:

Pokhrel, I., Kalra, A., Rahaman, M. M., & Thakali, R. (2020). Forecasting of Future Flooding and Risk Assessment under CMIP6 Climate Projection in Neuse River, North Carolina. Forecasting, 2(3), 323-346.

Conference Proceedings:

Kalra, A., Joshi, N., Pokhrel, I., Pradhan, S., Adhikari P., Xia, C, Gupta, R. (2020) Assessment of Floodplain inundation mapping of Davenport City in Iowa using CIVIL Geo-HECRAS. In World Environmental and Water Resources Congress 2021. (In Press).

Joshi, N., Bista, A., Pokhrel, I., Kalra, A., & Ahmad, S. (2019, May). Rainfall-Runoff Simulation in Cache River Basin, Illinois, Using HEC-HMS. In World Environmental and Water Resources Congress 2019: Watershed Management, Irrigation and Drainage, and Water Resources Planning and Management (pp. 348-360). Reston, VA: American Society of Civil Engineers.